TÉCNICO LISBOA

Analysis of the influence of mooring dynamics and hydrodynamic models on the response of floating offshore wind turbines using FAST

Philipp Hufnagel

Thesis to obtain the Master of Science Degree in

Energy Engineering and Management

Supervisors: Prof. Climent Molins

Prof. Luís Manuel de Carvalho Gato

Examination Committee

Chairperson: Prof. José Alberto Caiado Falcão de Campos

Supervisor: Prof. Luís Manuel de Carvalho Gato

Member of the Committee: Prof. Ricardo Balbino Santos Pereira

November 2017

Acknowledgements

I would like to thank all the people who contributed in some way to the work described in this thesis.

First and foremost, I would like to express my deepest appreciation to my thesis supervisor at Windcrete, Professor Climent Molins and to Pau Trubat (MSc.) for giving me the opportunity to write my thesis with them and for their support and help through every stage of the project. I am very thankful for their patience and willingness to answer my question and share their knowledge with me.

I would also like to thank my university supervisor from the Instituto Superior Técnico, Professor Luís Gato for giving me the chance to write about this truly interesting subject.

Thank you to my friend Ana for every coffee, supportive talk and help during this project. Furthermore, I want to thank my colleague Quentin for making the long office hours more entertaining.

Finally, my gratitude goes to my dear friends and colleagues from Entech, my friends in Germany and Barcelona and my family for suffering with me through this challenging time and for always having an open ear and calming words for me.

.

Abstract

In times of global warming, sustainable energy production becomes increasingly important. Floating offshore wind turbines are a relatively new technology which could help to solve the energy challenges of tomorrow. Aero-hydro-servo-elastic codes are used for the design and simulation of these turbines. The Offshore Code Comparison Collaboration projects (OC 3-5) aim to benchmark and verify these codes in order to further progress the field of offshore wind.

This thesis looks at various modules of the codes and highlights the differences in the used calculation models. In the first part, the importance of mooring dynamics is analyzed by reassessing a semisubmersible platform used in the OC4 project with both dynamic and quasi-static mooring models. Then, the influence and differences of calculating the hydrodynamic loads with either Morison's equation or a Potential flow model enhanced with the viscous terms from Morison's equation is examined based on the OC5 experiment. The last part aims to increase the application range of Morison's equation for platforms with large column diameters. A model to calculate the non-negligible diffraction loads for these platforms are introduced using MacCamy & Fuchs' diffraction theory. They are compared with the loads from airy waves predicted by Morison's equation on a vertical cylinder. The thesis closes with a review of the outcomes and an outlook for future works and applications.

Key words: Offshore design codes, mooring dynamics, hydrodynamic model, diffraction loads

Resumo

Sendo o aquecimento global um problema tão presente nos tempos que correm, a produção de electricidade de forma tecnologia sustentável está a tornar-se um tópico cada vez mais importante. A energia eólica offshore flutuante é uma relativamente nova com potencial para ajudar a solucionar alguns dos desafios energéticos do futuro. Para projectar e simular o comportamento destas turbinas, códigos aero-hidro-servo-elásticos são actualmente utilizados. Os projectos Offshore Code Comparison Collaboration (OC 3-5) têm como objectivo o benchmarking e verificação destes códigos, de modo a promover a progressão no campo da energia eólica offshore.

Este projecto analisa os diferentes módulos destes códigos e sublinha as diferenças nos diferentes modelos de cálculo utilizados. Na primeira parte, a importância da dinâmica do sistema de mooring é analisada estudando a resposta de uma plataforma semi-submersível, previamente estudada no projecto OC4, quando se utilizam modelos dinâmicos e modelos quase-estáticos. Posteriormente, duas formulações para modelar cargas hidrodinâmicas foram comparadas: a equação de Morison e um modelo de fluxo potencial aumentado com termos de viscosidade provenientes da equação de Morison. A influência e diferenças obtidas foram examinadas com base nos resultados do projecto OC5. A última parte tem como objectivo aumentar o intervalo de aplicação da equação de Morison para plataformas com colunas de grandes diâmetros. Um modelo para calcular cargas de difração não-negligenciáveis foi introduzido utilizando a teoria de difração de MacCamy e Fuchs. Estas cargas foram comparadas com as cargas causadas por ondas

lineares num cilindro vertical calculadas com a equação de Morison. Finalmente, uma revisão dos resultados e uma projeção sobre trabalho e aplicações futuras é apresentada.

Palavras-chave: Códigos de design offshore, dinâmica de mooring, modelos hidrodinâmicos, cargas de difração

Table of contents

Abbreviations

WWEA	World wind energy association
NREL	National Renewable Energy Laboratory
FAST	Fatigue, Aerodynamics, Structures, and Turbulence Code
WindPACT	Wind Partnerships for Advanced Component Technology
RECOFF	The Recommendations for Design of Offshore Wind Turbines
DOWEC	Dutch Offshore Wind Energy Converter
ME	Morison's equation
PF	Potential Flow
OC	Offshore Code Comparison Collaboration
RAO	Response Amplitude Operator
MBS	Multi body system
DOF	Degree of freedom
MSL	Mean sea level
IEC	International Electrotechnical Commission
PSD	Power Spectral Density

Table of Figures

Tables

1 Introduction

Undeniably, we live in a time of global warming. The temperature is rising, the polar ice caps are melting more rapidly than predicted and the sea level is rising. Dangerous, irregular weather patterns and climate catastrophes like draughts, floods, and wildfires are occurring more frequently. Thirteen of the fourteen hottest years since the beginning of climate reports have been observed within the last seventeen years [1]. To avoid a further escalation of these problems, a drastic and fundamental change from our carbon-based society towards a more sustainable form of living is necessary. The emission of greenhouse gases, which is still rising, needs to be significantly reduced. One way to contribute to this transformation is to switch from fossil fuel-based energy production to climate-neutral, renewable energy sources [2].

To achieve this goal, the wind power industry is a valuable key factor to provide sustainable, emission-free energy. In the last two decades, the wind industry has established itself as a major player in the energy mix. The installed capacity has, according to the World Wind Energy Association (WWEA), reached over 54 GW in 2017, thus being able to provide around 5% of the global electricity demand In 2015 a total investment of 316 billion USD was made and thousands of jobs were created worldwide. [3].

Due to significant cost reductions in turbine manufacturing and at the same time less and less available installation area, offshore wind farms are on the rise. In 2016, over 338 new offshore turbines with 1.5 GW capacity were installed in Europe alone, with an expected total offshore capacity of 25 GW in 2020. The average water depth for installed turbines increased to 29m in a distance of 44 km to the shore. The first 8MW turbines have been installed, pushing the average rated turbine power to 4.8 MW [4]. All of these turbines are, as of now, bottom-fixed systems, made for shallow water depths. If this trend continues, floating systems, which can utilise the superior wind conditions further off the coast, will be worth considering. The construction of the first 30 MW windfarm of this type, the Hywind project from Statoil in Aberdeenshire, Scotland, has started in 2017. It features 5 spar type platforms mounted with 6 MW turbines anchored in water depths of around 100 metres. This project will pave the way towards a lucrative future market for floating offshore farms. Especially in proximity to major costal metropolitan areas, the potential for these type of systems is huge due to the minimised transmission losses [5].

The key to success for deep-water floating offshore wind turbines is the development of reliable and sophisticated tools to design and evaluate these systems. According to the IEC 61400-3 design standard for offshore wind system, a thorough load analysis needs to be performed before a turbine can be commissioned. The tools used for this kind of assessments are aero-hydro-servo-elastic simulation tools, like the Fatigue, Aerodynamics, Structures, and Turbulence (FAST) code from the National Renewable Energy Laboratory (NREL).

In this thesis, the modeling capacity of FAST compared to other codes used for floating offshore systems is analysed. It reviews the results from the Offshore Code Comparison Collaborative (OC3) project, a joint project between research centers, companies and universities, with the goal to benchmark different offshore codes, and compare them with the results of the newest version of FAST (V8.16).

Furthermore, it analyses the influence of dynamics in the calculation of the mooring loads for the semisubmersible platform used in the OC4 project, by reproducing selected load cases of the OC4 study with both quasi-static and dynamic mooring models.

As a third step, it deals with the establishment of a FAST model for the OC5 project, which aims to verify the theoretical results of earlier projects by providing experimental data from a model test. The influence of the hydrodynamic modelling approach is the focus of this part of the thesis, comparing a combination of Potential Flow and Morison's Equation with only Morison's equation. Differences in the Response Amplitude Operators and the occurring loads on the tower are analyzed.

Finally, the question whether the inclusion of MacCamy 's & Fuchs's wave diffraction theory enables the use of Morison's equation for platforms with a large diameter-to-wavelength ratio is examined.

A summary and a conclusion of the findings complete the thesis.

2 Background

2.1 Offshore wind Concepts

There are many different types of offshore wind turbines currently employed or under development. Depending on water depth, shore type and environmental conditions the systems can be categorised into two groups, bottom-supported and floating structures [6].

2.1.1 Bottom-supported systems

Bottom-supported structures are either compliant structures or fixed to the seabed. Fixed systems consist of a rigid tower with a foundation. There are several design approaches like monopiles, jack-up rigs which are mobile platforms that can elevate themselves above the waterline after their legs have been rammed into the ground or fortified gravity platforms that use concrete ballast to keep the steel tower attached to the seabed. The most common design in the wind industry is a jacket structure which features a steel truss tower on top of tubular legs which are anchored with piles to the floor. They are suitable for water depths of up to 100 meters. The tower is stiff which keeps the natural frequency of the system above the energetic wave frequencies as well as wind frequencies which makes this concept a promising option for wind turbines in shallow water [7].

Compliant towers are connected to the sea floor with a piled foundation which supports a flexible truss tower allowing them to move freely with the waves, current and wind. Their typical employment depth is between 300 and 800 meters. These systems are sometimes enhanced with mooring lines. They rely on the restoring buoyancy force to maintain their stability after lateral movements and avoid resonance problems by operating at natural frequencies far below the energetic wave frequencies[7]. Compliant systems are currently not regularly employed for offshore wind turbines for several reasons: the tower becomes too stiff for shallow water depths, which puts the natural frequency dangerously close to the wave frequencies and energetic wind frequency that are in the lower spectrum, leading to resonance problems. Furthermore, the turbine-wind interaction results in huge loads on the upper part of the tower, which is a unwanted effect in combination with the very flexible design [8].

2.1.2 Floating systems

If the water depth exceeds a certain limit, bottom-supported systems are no longer employable. Therefore, floating system that are tethered to the floor with mooring lines are used. They can be divided into neutrally, and positively buoyant platforms.

The dominant concepts for neutrally buoyant platforms are semi-submersible systems, and spar buoys. They can move in all six directions of movements (to a certain degree) without being restricted by the mooring lines. Their draft is determined by the balance between gravity and buoyancy [9]. Semi-submersible platforms usually consist of a deck which is supported by three to four pillars connected with pontoons and braces. They can be filled with ballast to adjust the draft of the system. Their centre of

gravity is fairly above the centre of buoyancy. Hence the stability needs to be achieved by enlarging the water surface area. The heave motion is restricted by adding plates on the bottom of the columns which - according to Archimedes's law – prevent the movement. In pitch and roll direction, the platform is regulated by its restoring moments while surge, sway and yaw have to be stabilised with the mooring system. Spar buoys on the other hand are slender, cylindric structures which use heavy ballast in the bottom part to achieve a centre of gravity which is lower than the centre buoyancy which makes the system intrinsically stable. They rely on the buoyancy to stabilise heave movements and on a high metacentric height to prevent kipping in roll and pitch direction. In yaw direction, there is almost no hydrodynamic excitation. But due to the wind influence on wind turbines, the yaw displacement has, as well as surge and sway motions, to be controlled by mooring lines [10].

Positively-buoyant platforms are fixed with a pretension in the mooring lines into a position which is lower than their natural draft. In this setup, the buoyancy force is exceeding the gravity force, hence the system is positively-buoyant. Due to the mooring line setup, these structures are also called "Tension Leg Platforms (TLP)". The pretension restricts the movement in heave direction, enabling only five degrees of freedom [9]. Stability in the remaining directions is achieved in the same way as it is for the semisubmersible platform [10].

2.2 Movements of floating structures

Floating vessels move with the influence of waves and wind. These movements can be described by six degrees of freedom. Movements along the axis x_b are called *surge*, in lateral y_b direction *sway* and vertical along z_b *heave*. Rotations around these axis are measured positive in clockwise direction and are called roll, pitch and yaw (Φ,θ and ψ respectively) [6]. The available degrees of freedom for a vessel are shown in figure 1. All values given in this thesis are measured from the centre of a fixed coordinate system. In the case of floating offshore turbines, additional degrees of freedom for the turbine complement the model. The software used in this thesis, FAST, considers 17 different degrees of freedom:

- First flapwise blade mode
- Second flapwise blade mode
- First edgewise blade mode
- Rotor-teeter (unused for 3 blades)
- Drivetrain rotational-flexibility
- Generator
- Nacelle yaw rotation
- First fore-aft tower bending-mode
- Second fore-aft tower bending-mode
- First side-to-side tower bending-mode
- Second side-to-side tower bending-mode
- Platform horizontal surge translation

- Platform horizontal sway translation
- Platform vertical heave translation
- Platform roll tilt rotation
- Platform pitch tilt rotation
- Platform yaw rotation

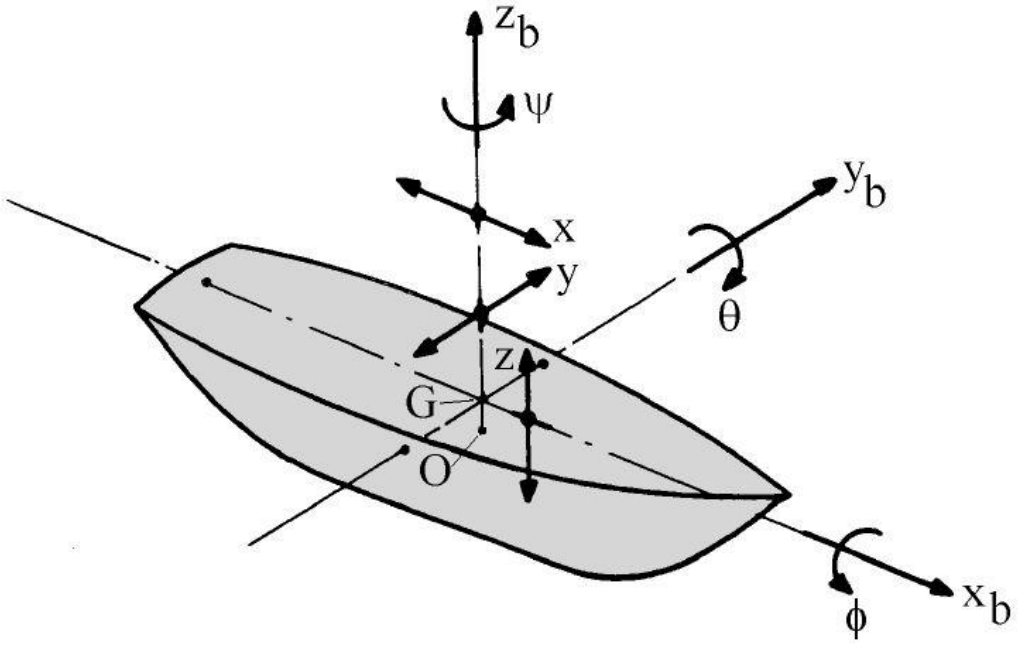

Figure 1: Degrees of freedom of a floating vessel [6]

2.3 Loads on floating offshore turbines

A floating wind turbine is subjected to a multitude of hydrodynamic and aerodynamic loads from wind and waves. The dominant forces working on floating systems are caused by aero- and hydrodynamic effects. They can be predicted with design codes like FAST (cf. next chapter). Due to the complexity of the influencing factors, these codes have to make assumptions and simplifications. The next subchapters provide an overview over the most important load sources and simplifications performed by FAST.

2.3.1 Hydrodynamic loads

The hydrodynamic loads on a floating structure can be divided into three groups, viscous forces, wave excitation and radiation due to the motion of the platform. The calculation of these forces and the connected hydrodynamic behaviour can be performed in different ways. One of the goals of the OC projects is the verification and legitimation of these approaches. Therefore, a wide spectrum of combinations and solving models are tested. The codes used by the participants of the projects are divided into three groups. Either potential flow theory enhanced with Morison's equation or a quadratic drag term

or solely Morison's equation is used. In the following first Potential Flow and then Morison's equation is explained.

The potential flow theory is suitable for floating structures that are relatively large compared to the incoming wavelength. It regards the flow as an inviscid and incompressible fluid attached to the object which allows the use of this simplified theory [9]. It was developed for stationary objects which means the motion of the platform must be negligible compared to its size which often is not given, especially for systems with catenary mooring lines [11]. In order to make potential flow theory valid and applicable in a wider range of conditions, external tools like WAMIT are used. WAMIT uses a "*three-dimensional numerical-panel method in the frequency domain*"[12] that enables the linear potential flow theory to deal with radiation and diffraction. Radiation loads occur due to the oscillation of the platform that emits waves outwards while diffraction loads are the loads inflicted upon the platform by the incoming waves that are scattered by the body. Together with WAMIT, 1st and 2nd order diffraction (Froude-Krylov and scattering) can be evaluated. The total hydrodynamic loading on the system can be seen as a superposition of the two effects - this principle is represented in figure 2:

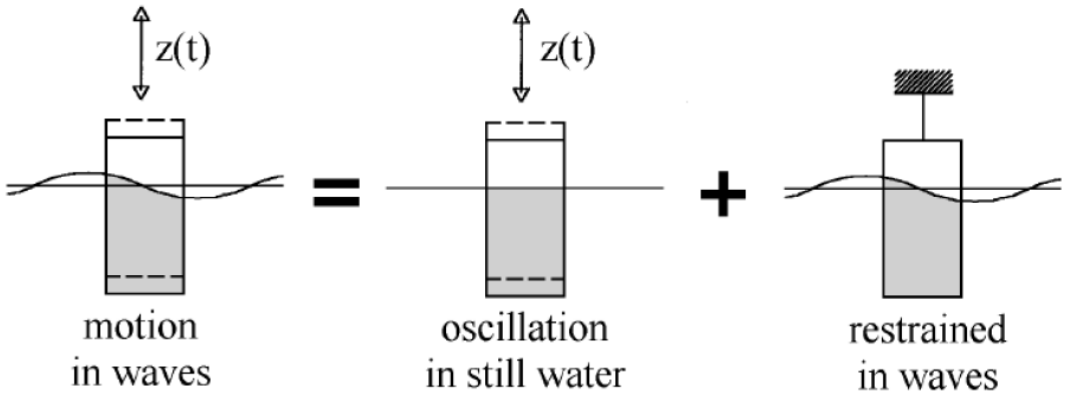

Figure 2: Hydrodynamic loads on a cylinder

A drawback of the theory is that it is not valid for severe sea conditions or smaller structures where the effects of the occurring flow separation must be taken into account. The occurring viscous drag forces are not captured by the potential flow theory. However, this can be addressed by either including additional damping for all degrees of freedom to account for quadratic drag or by using parts of Morison's equation.

Furthermore, not all codes used by the participants are capable to work with the potential flow theory and are instead based solely on the Morisons's equation. Morison's equation is a semi-empirical model for the estimation of hydrodynamic loads. It states that the force on the structure will be a sum of an inertial force (from potential flow theory) and a viscous quadratic drag force[6]. For a fluid with the density ρ and a cylinder with the diameter D, the resulting force per unit length is:

$$F(t) = \frac{\pi}{4}\rho C_m D^2 \cdot \dot{u}(t) + \frac{1}{2}\rho C_d D \cdot u(t)|u(t)| \quad (1)$$

The first term, proportional to the acceleration $\dot{u}(t)$ is the inertia term and the second, proportional to the squared velocity $u(t)|u(t)|$ is the drag term, with C_m and C_d being the empirical inertia and drag coefficients. The inertia term is the sum of the Froude-Krylov force and the hydrodynamic mass force. The Froude-Krylov force results from the wave pressure acting on the submerged surface part of the structure. [6]. If the hydrostatic forces and dynamic pressure loads are accounted for, Morisons's equation is able to describe the complete hydrodynamic loads of the structure. The results can be further refined by wave stretching methods or by carefully applying the forces up to the instantaneous water surface elevation of the platform[12].

If potential flow theory or Morison's equation should be used can be estimated by the comparison of dimensionless parameters, namely the Keulegan-Carpenter number, the Reynolds number, and the diameter-to-wavelength ratio. They give information about the importance of drag forces over inertial forces, the ratio of inertial to viscous forces as well as the influence of diffraction [13]. Morison formulation can be used to estimate hydrodynamic loading whenever the effects of diffraction and radiation damping are negligible. Diffraction is dominated by inertia loads when the diameter of the structure is small considered to the wavelength (usually, the rule of $\lambda > 5D$ is used). If the drag term dominates damping, the radiation damping can be ignored, which is valid if the motions of the cylinder are small [14]. For the semisubmersible platform analysed in this thesis, both solutions provide valid and sufficiently exact results for most load cases.

2.3.2 Aerodynamic loads

Similar to hydrodynamic loads, the aerodynamic forces can be described by dividing them into several individual components. The source of these loads is the incoming wind interacting with turbine blades, tower and platform. The wind is composed of a steady, non-fluctuating part, and a turbulent part like gusts. Additionally, periodic but dynamic elements play a role, for example wind shear and the build-up of a stagnation layer in front of the tower.

2.3.2.1 Steady aerodynamic loads

Steady loads are caused by the interaction of the mean wind on turbine, tower, and platform. The thrust force inflicted on the rotor has the strongest effect. The rotor is modelled as an actuator disc which means the airflow before and after the rotor is uniform. Due to the deceleration of the air by the rotor, a pressure gradient which depends on the mean wind speed forms. According to Bernoulli's law this gradient results in a thrust force on the rotor.

$$F_T = A\left(p_{right\ before\ disc} - p_{right\ after\ disc}\right) = \frac{1}{2}\rho A\left(u_{before}^2 - u_{after}^2\right) \tag{2}$$

Hereby A is the swept rotor area and ρ the air density. Thus, the only variable is the difference between the wind velocity far in front of the rotor and after passing the rotor. Furthermore, the mean wind will induce a constant drag force on the other parts of the system like the tower and the floating platform [15].

In real offshore systems, the steady loads have to be compensated by adjusting the mooring tension according to expected wind speeds [16].

2.3.2.2 Turbulence loads

The unsteady parts of a wind field are called turbulences. They are time-dependent, stochastic, and randomly occurring effects. Their wind speed deviates from the mean wind speed without affecting the mean. Consequently, the most impactful events for offshore wind turbines are hereby strong gusts, short periods of high local wind velocity which inflict high forces on the whole rotor or only parts of the turbine blades. These cause stall effects, rapid load changes and immense fatigue and ultimate loads which have a huge influence on the fatigue lifetime of turbines. In particular at offshore sites these events occur more often and need to be considered in the design of the system [6].

2.3.2.3 Periodic aerodynamic loads

Next to turbulences, there are also other dynamic loads occurring on the rotor blades. Effects such as wind shear, constant off-axis wind, or deceleration of the wind in front of the tower create periodically reappearing influences on the aerodynamic loads. Shear is the change in windspeed with height due to the surface roughness. It can be described by the vertical power shear law:

$$v(z) = v_{ref}\left(\frac{z}{z_{ref}}\right)^{\propto} \tag{3}$$

v is the windspeed, z the altitude and α the shear exponent. Although the shear exponent is only 0.14 for typical offshore conditions, the difference in the wind speed between the tip of the blade at the highest point and the lowest point of rotation is considerable [17]. The load fluctuation due to shear is experienced by each blade once per rotation (and therefore with a frequency of 1P and multiples). Another effect is the build-up of a boundary layer of air around the tower. The tower is an obstacle for the airflow which leads to a deceleration of the air in front of it. The blades pass this zone of reduced wind velocity once per rotation and are therefore excited with a frequency of 1P and multiples of 1P. The stands hereby for “per rotation”. The tower and nacelle are exposed to this influence as well with a period of 3P, 6P, 9P…These components might cancel each other out but also build up. To avoid dangerous resonance effects, turbines are designed with natural frequencies far outside of the range of these frequencies [16].

2.3.3 Mooring line dynamics

The mooring system’s main responsibility is to keep the platform fixed to its position on the seabed. Two substantially different types of moorings can be differentiated. Taut moorings, also called tension lines, are equipped with a winch to control together with the weight of the line and the buoyancy of the structure the tension in the line. Slack mooring systems in comparison achieve the tension in the line only with the weight of the line itself. In slack systems, parts of the line can be resting on the seabed which adds another level of complexity. Mooring systems are designed to provide a dampening of the wave and wind induced

motions of the structure and are therefore essential for the stability of some platforms (e.g. Tension Leg Platforms)[18].

Mooring systems in shallow water can be sufficiently modelled with a quasi-static approach due to the limited total mass of the lines and the small motions of the system. This allows for the correct prediction of the restoring moments on the platform. Although serious drag forces along the lines can occur, it is common practice to omit the dynamic behaviour for those water depths. The achieved results are still sufficiently exact.

With rising water depth, the dynamic behaviour of the lines, like line inertia, drag or vortex shedding, gains increasing importance and cannot be neglected anymore. There are several ways to implement the dynamic nature of the mooring system. The most promising approach is to divide the line into several discrete, rigid elements which are connected by spring-damper systems. This method is called multibody system (MBS). It allows for an implementation of the dynamic mooring codes into existing offshore codes. The spring-damper systems between the bodies model extensional and rotational stiffness and the accordant damping. Depending on the material and the structure of the line this simplification has greater or smaller impact on the results. The interaction with the seabed is simultaneously modelled as a combination of springs and dampers. The only enabled degrees of freedom of the bodies are the elongation along the line as well as the bending of the line. The twist of the line as well as elongation orthogonal to the line axis are omitted from the model. Figure 3 shows a visualisation of these assumptions [11].

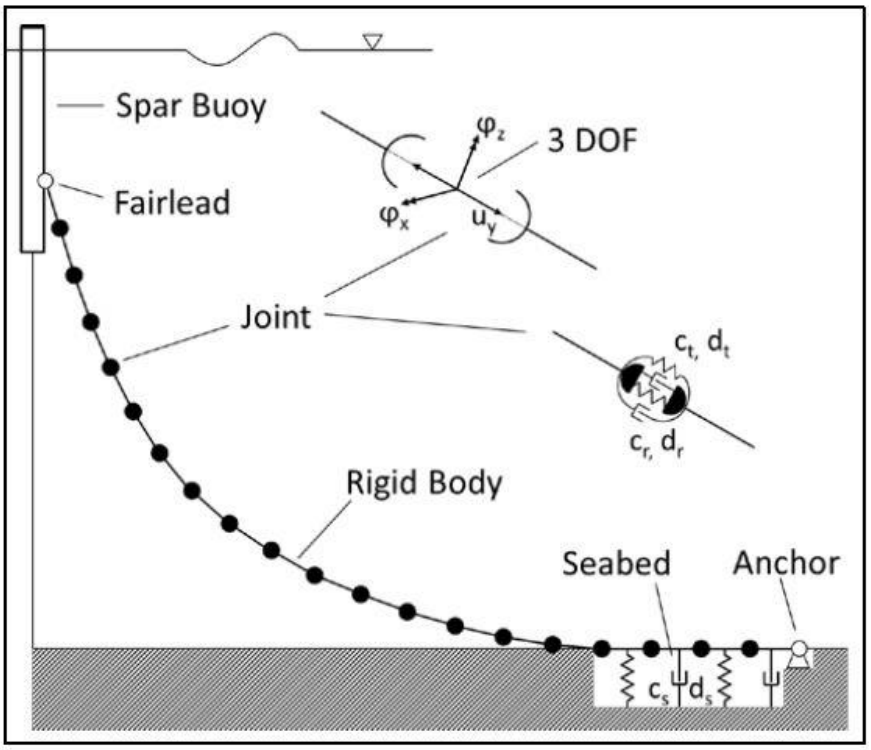

Figure 3: Catenary mooring systems [11]

2.4 FAST

The design of floating offshore wind systems poses a significant challenge due to the variety of influences that have to be considered. One approach for this complex problem are aero-hydro-servo-elastic codes. They combine established codes for onshore turbines with recent models that calculate the loads from incoming waves and current, hydrodynamics and foundation dynamics. Several different code solutions for these intricate systems exist [19]. One of them is the Fatigue, Aerodynamics, Structures, and Turbulence Code (FAST), which was developed and designed by Jonkman and Buhl of the NREL. The version of FAST used for all simulations performed in this report is version 8.16. It incorporates several individual stand-alone codes to model the complete aero-hydro-servo-elastic response of a variety of offshore floating wind turbines. An overview of these individual modules and their interconnection is shown in figure 4:

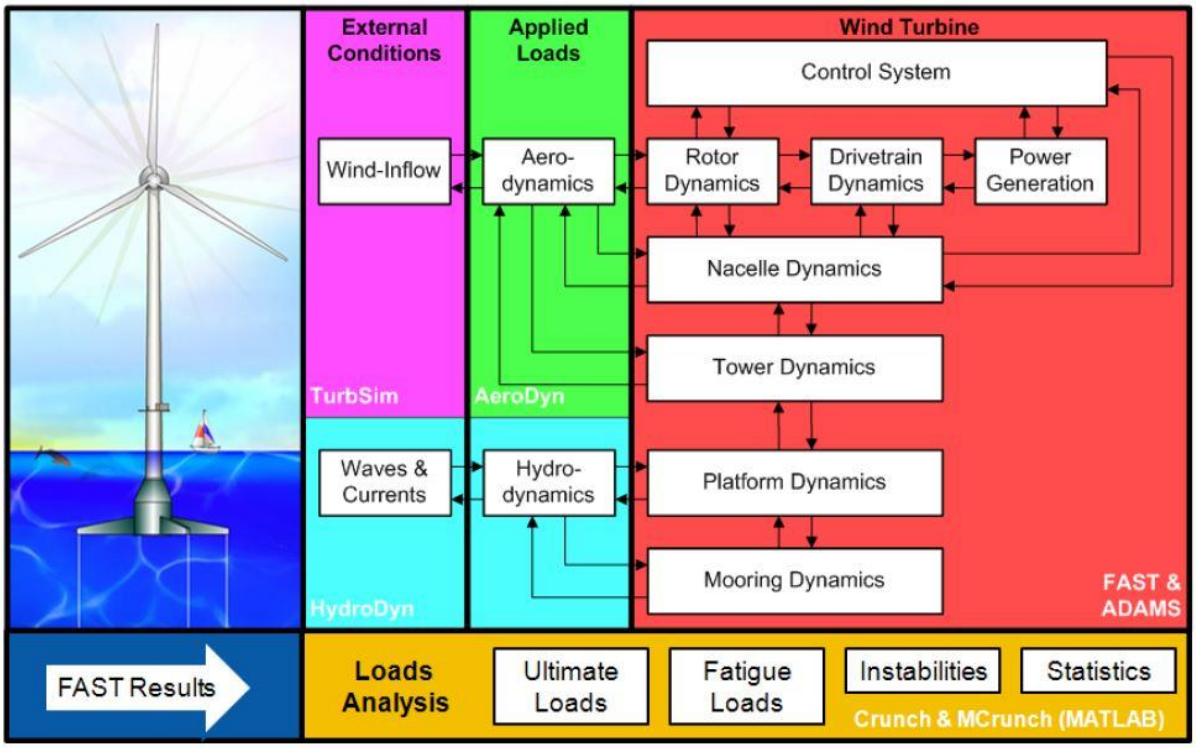

Figure 4: Modules of FAST [16]

AeroDyn

FAST utilises the code AeroDyn to calculate the aerodynamic loads on blades and tower in the time domain. It is possible to analyse turbines with one to three blades. Based on input parameters from FAST like the instantaneous structural position, detailed information about the analysis nodes in the tower, hub, and blades, AeroDyn is able to calculate the effect of the rotor wake with induction factors gained through a sophisticated Blade-Element/Momentum theory model. This is supported by empirical corrections to accommodate for tip and hub losses. Furthermore, the blade airfoil aerodynamics are

computed taking into account effects like the influence of the tower on the airflow, stall delay or a turbulent wake state [20].

HydroDyn

The hydrodynamic loads on a structure are analyzed with the tool HydroDyn. It works in the time domain and is able to generate its own wave data or use externally generated wave fields as an input. The waves can be regular or stochastic and uni- or multi-directional. Either a potential flow theory, a strip-theory, or a combination of both is used. HydroDyn is capable of calculating first order (linear Airy) and second order wave effects. Linear radiation including added mass and damping contributions, viscous drag and sea current loading are also considered by the code [21].

SubDyn

The module SubDyn enables the modeling of bottom-fixed structures like monopiles, tripods, jackets, and other non-floating systems. It uses a linear frame finite-element beam model (LFEB) in conjunction with the Craig-Bampton(C-B) method to minimize the necessary number of nodes and therefore reduce the solver time. Together with HydroDyn it outputs coupled hydro-elastic loads as well as the internal reaction of the elements of the support structure [22].

ServoDyn

ServoDyn is the control unit of FAST and is taking care of the operation of the turbine. It includes control and electrical-drive models to administer the blade pitch, the generator torque, and the yaw movements of the nacelle. Different break systems can be utilized like high-speed shaft and blade-tip brakes to ensure a safe operation under all conditions. ServoDyn can be supported by external Fortran subroutines or Bladed-style dynamic link library (.DLL) files or be connected to MATLAB via a Simulink interface [23].

ElastoDyn

The ElastoDyn module calculates the resulting displacements, velocities, accelerations, and reaction loads on the system due to the aero- and hydrodynamic loads, the controller input and the substructural influence of the seafloor. It enables output in 24 degrees of freedom for different turbine configurations [24].

IceFloe/IceDyn

IceFloe and IceDyn make it possible to analyze the influence of surface ice on offshore structures. If the offshore wind industry continues its expected growth, some turbines will be placed in regions of the sea where ice buildup is possible. Thus, these modules are included in FAST to observe the effect these extreme climate conditions have on the systems [25].

3 OC4 Phase II: Semisubmersible Floating System

3.1 Overview

The Offshore Code Comparison Collaboration Continuation project (OC4) is the continuation of the OC3 project, a joint collaboration of several research institutes, universities and industrial corporations around the world. Its goal is to verify and develop the simulation tools to design and analyze offshore wind turbine systems. The interaction of different wind and wave conditions, exert complex dynamic loads on offshore systems. To predict the responses of these systems, the conventional codes for the analyzation of land-based turbines must be combined with hydrodynamics, waves and current theory and foundation dynamics of the platform. The resulting codes are highly sophisticated and therefore requires lengthy and thorough testing. This is done in the OC3 and OC4 studies by benchmarking the different codes of the participants with different support structures and varying external conditions and comparing the results [13].

The second phase of the OC4 project regarded here uses the NREL 5MW turbine mounted on a semisubmersible floating platform. The platformed was initially developed for the DeepCWind project [12]. DeepCWind is a joint cooperation between numerous partners with industrial and academic background to generate test data for benchmarking offshore wind tools. It utilizes a 1/50 scaled model which is tested under varying conditions in a wave tank [26]. The system can be seen in figure 5:

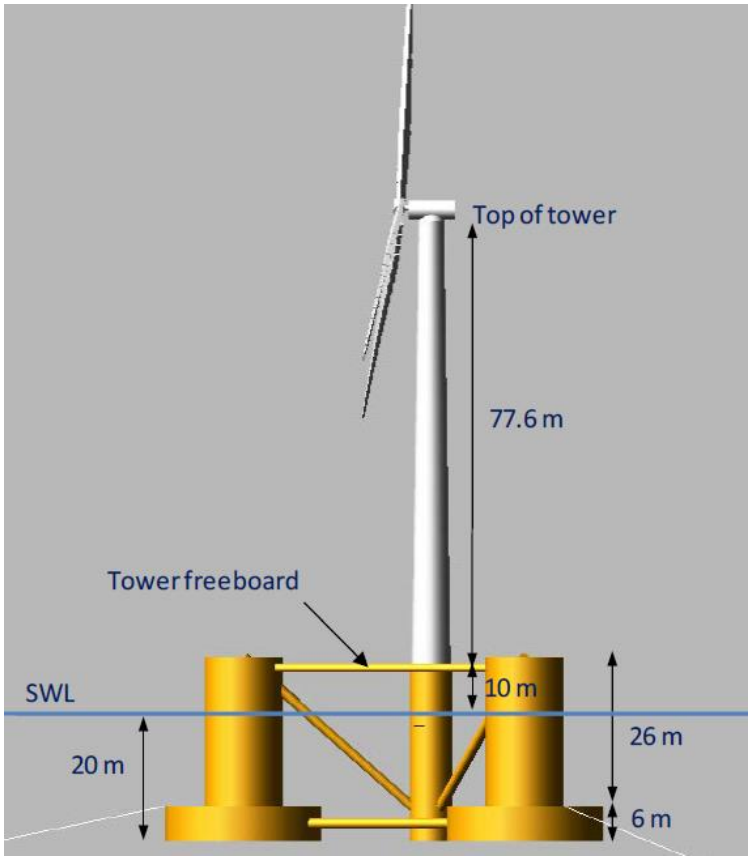

Figure 5: OC4 semisubmersible with NREL 5MW turbine

Several load cases are examined with a focus on the calculation model of the mooring system. For this purpose, every analysis is performed with a dynamic mooring model via MoorDyn as well as a quasi-static approach through MAP++. The aim is to obtain information about the importance of the inclusion of dynamic behaviors like line inertia, drag or vortex shedding for platforms of this type and in water depths around 200 meters.

3.1.1 Floating support structure

The second phase of the OC4 project utilizes a semisubmersible platform as shown in figure 5. These platforms consist of a deck, columns, and pontoons. They have, in comparison to a spar design, a center of gravity higher than their center of buoyancy. The restoring moment of the offset columns keeps the platform stable. While deployed, the pontoons of the platform are filled with ballast, which changes the platform's main means of flotation from the pontoons to the columns [9]. The design used for the second phase of OC4 consists of three offset columns connected to a central column with pontoons. The bottom parts of the offset columns are connected to base columns with a wider diameter to suppress heave, and to a smaller degree pitch and roll motions. The ballast is realized by partly filling the three offset columns with water. Neither the pontoons nor the main columns are filled with water. This results in a platform draft of 20m and a weight including the ballast of $1.35 \cdot 10^7\ kg$. Further geometrical details are listed in table 1:

Table 1: Geometry of the OC4 Semisubmersible Platform

Parameter	Length
Depth of platform base below SWL (total draft)	20 m
Elevation of main column (tower base) above SWL	10 m
Elevation of offset columns above SWL	12 m
Spacing between offset columns	50 m
Length of upper columns	26 m
Length of base columns	6 m
Depth to top of base columns below SWL	14 m
Diameter of main column	6.5 m
Diameter of offset (upper) columns	12 m
Diameter of base columns	24 m
Diameter of pontoons and cross braces	1.6 m

The floater is anchored in the seabed with three catenary lines which are placed symmetrically with 120 degrees offset between the lines. The cables have an unstretched length of 835.5m with a diameter of 0.0766 m.

The control system of the turbine is a modified version of the one used in the OC3 Hywind project. During the OC3 tests it became clear that the used pitch-to-feather control can in combination with wind speed

above rated speed lead to negative damping and resonance in offshore structures. To avoid this from happening, the controller was adapted to only allow for positive damping.

Further details for the floating system can be found in the NREL/TP-5000-60601 report by A. Robertson et al [26].

3.1.2 Turbine properties of NREL 5MW Turbine

To ensure a comparability of the various studies performed with FAST, the similarity of the examined turbine has to be guaranteed. Therefore, a standardised design for the turbine was chosen. The so called "NREL offshore 5 MW baseline wind turbine" is based on the Multibrid M5000 and REpower 5 MW turbines as well as the conceptual models from various projects (namely WindPACT, RECOFF, and DOWEC)

It is a regular three-bladed turbine suitable for offshore usage. The blades have a radius of 63 meters and sit at a hub height of 90 m. They consist mostly of fiberglass with eight distinct airfoil shapes along their radius (cylindric shapes close to the hub followed by DU shapes in the midsection and NACA shapes towards the tip).

The rated rotor speed is 12 rpm with a rated power output of 5 MW. It is equipped with a dual control system of a generator-torque controller below rated power and a blade-pitch-to-feather controller to slow the turbine above the operation point[14]. The chosen design parameters can be seen in table 2:

Table 2: Properties of the NREL 5 MW turbine [27]

Parameter	Value
Rated Power	5 MW
Rotor Orientation, Configuration	Upwind, 3 Blades
Control System	Variable Speed, Collective Pitch
Drivetrain	High Speed, Multiple-Stage Gearbox
Rotor, Hub Diameter	126 m, 3 m
Hub Height	90 m
Cut-In, Rated, Cut-Out Wind Speed	3 m/s, 11.4 m/s, 25 m/s
Cut-In, Rated Rotor Speed	6.9 rpm, 12.1 rpm
Rated Tip Speed	80 m/s
Overhang, Shaft Tilt, Precone	5 m, 5º, 2.5º
Rotor Mass	110,000 kg
Nacelle Mass	240,000 kg
Tower Mass	347,460 kg
Coordinate Location of Overall CM	(-0.2 m, 0.0 m, 64.0 m)

Further elaboration on the design choices for the turbine can be found in NREL/TP-500-41958[27].

3.1.3 Participants and used codes

The collaboration for OC4 includes, as mentioned before, various international members under the leadership of the NREL. Table 3 gives an overview of the participants and the respective codes they used.

Table 3: Participants and used codes in OC4 [13]

Code	Code Developer	OC4 Participant	Structural Dynamics	Aerodynamics	Hydrodynamics	Mooring Model
FAST	NREL	NREL, CENTEC, IST, Goldwind, CSIC	T: Mod/MB P: Rigid	(BEM or GDW)+DS	PF + QD + (QTF)	QS
FAST v8	NREL	NREL	T: Mod/MB P: Rigid	(BEM or GDW)+DS	PF + ME	QS
CHARM3D+ FAST	TAMU+ NREL	ABS	T: Mod/MB P: Rigid	(BEM or GDW)+DS	PF + ME + (MD + NA) + (IP + IWL)	FE/Dyn
OPASS+ FAST	CENER+ NREL	CENER	T: Mod/MB P: Rigid	(BEM or GDW)+DS	PF + ME	LM/Dyn
UOU+FAST	UOU+NREL	University of Ulsan	T: Mod/MB P: Rigid	(BEM or GDW)+DS	PF + QD	QS
Bladed	GH	GH, CGC, POSTECH	T: Mod/MB P: MB	(BEM or GDW)+DS	ME + (IWL+ IP)	QS
Bladed Advanced Hydro Beta	GH	GH	T: Mod/MB P: MB	(BEM or GDW)+DS	PF + ME + (IWL)	QS
OrcaFlex	Orcina	4Subsea	T: FE P: Rigid	BEM, GDW, or FDT	PF + ME	LM/Dyn
HAWC2	DTU	DTU	T: MB/FE P: MB/FE	(BEM or GDW)+DS	ME	FE/Dyn
hydro-GAST	NTUA	NTUA	T: MB/FE P: MB/FE	BEM or FWV	PF + ME + (IP)	FE/Dyn
Simo+Riflex+ AeroDyn	MARINTEK+ NREL	CeSOS	T: FE P: FE	(BEM or GDW)+DS	PF+ME	FE/Dyn
Riflex-Coupled	MARINTEK	MARINTEK	T: FE P: Rigid	BEM+FDT	PF + ME + (IWL)	FE/Dyn
3Dfloat	IFE-UMB	IFE	T: FE (co-rotated) P: FE	BEM+FDT	ME + (IWL)	FE/Dyn
SWT	SAMTECH	SAMTECH & IREC	T: FE+Mod/MB P:FE+Mod/MB	BEM or GDW	ME + (IWL)	FE/Dyn
DeepLinesWT	PRINCIPIA-IFPEN	PRINCIPIA	T: FE P: FE	BEM+DS	PF + ME + (MD + QTF/NA) + (IP + IWL)	FE/Dyn
SIMPACK+ HydroDyn	SIMPACK	SWE	T: Mod/MB P: Rigid	BEM or GDW	PF + QD	QS
CAsT	University of Tokyo	University of Tokyo	T: FE W: FE	BEM	ME	QS
Wavec2Wire	WavEC	WavEC	T: N/A P: Rigid	N/A	PF + QD	QS
WAMSIM	DHI	DHI	T: N/A P: Rigid	N/A	PF + QD	QS

T = turbine P = platform Mod = modal MB = multi-body FE = finite element N/A = not applicable	BEM = blade-element/momentum GDW = generalized dynamic wake DS = dynamic stall FDT = filtered dynamic thrust FWV = free-wake vortex	PF = potential flow theory ME = Morison eq. MD = mean drift QTF = quadratic transfer function NA = Newman's approximation IP = instantaneous position IWL = instantaneous water level QD = quadratic drag	QS = quasi-static Dyn = dynamic LM = lumped mass

While the codes for structural dynamics and the aerodynamics are well established, there are several approaches for the calculation of the mooring model and the hydrodynamics. Most of the codes use either blade-element/momentum theory or a generalized dynamic wake model with dynamic stall. The following chapters deals in detail with the differences in the modelling of the mooring system and the hydrodynamics.

3.2 Analysis

In order to verify and benchmark the various codes, 21 tests with increasing complexity and changing external conditions are performed. The first group concerns the system identification, performing eigenanalyses, static equilibrium tests and free decay tests. Group number two examines the turbine's behaviour under changing wave conditions without the influence of wind in so called inverse pendulum

tests. The last series of tests takes a look at the response of the system for different realistic wave and wind conditions [13]. The hydrodynamics in all tests performed for the OC4 part of this thesis are calculated with potential flow theory enhanced by Morison's equation, as indicated in table 3 for FAST v8. A focus in this part of the thesis is the difference between the results of a dynamic modelling of the mooring system with MoorDyn compared to the quasi-static approach used by the original participants of the study. This gives valuable information about the importance of dynamic loads on the mooring lines. For this reason, all analyses except the static equilibrium test are performed with both approaches, labelled as DM and QS respectively.

3.2.1 Static equilibrium test

Static equilibrium tests examine the behaviour of the system without external excitation. The wind inflow is zero, the aerodynamics are not considered and the wave input is set to still water conditions. All degrees of freedom are enabled. Of interest are the static equilibrium positions of the platform after the transients. As figure 6 shows, most codes agree quite well in all six directions of motion. The BLADED code utilised by GH overpredicts the surge and heave movement slightly relative to all the other codes. The results obtained with the newest FAST version 8.16 used in this thesis, match the results from the initial study.

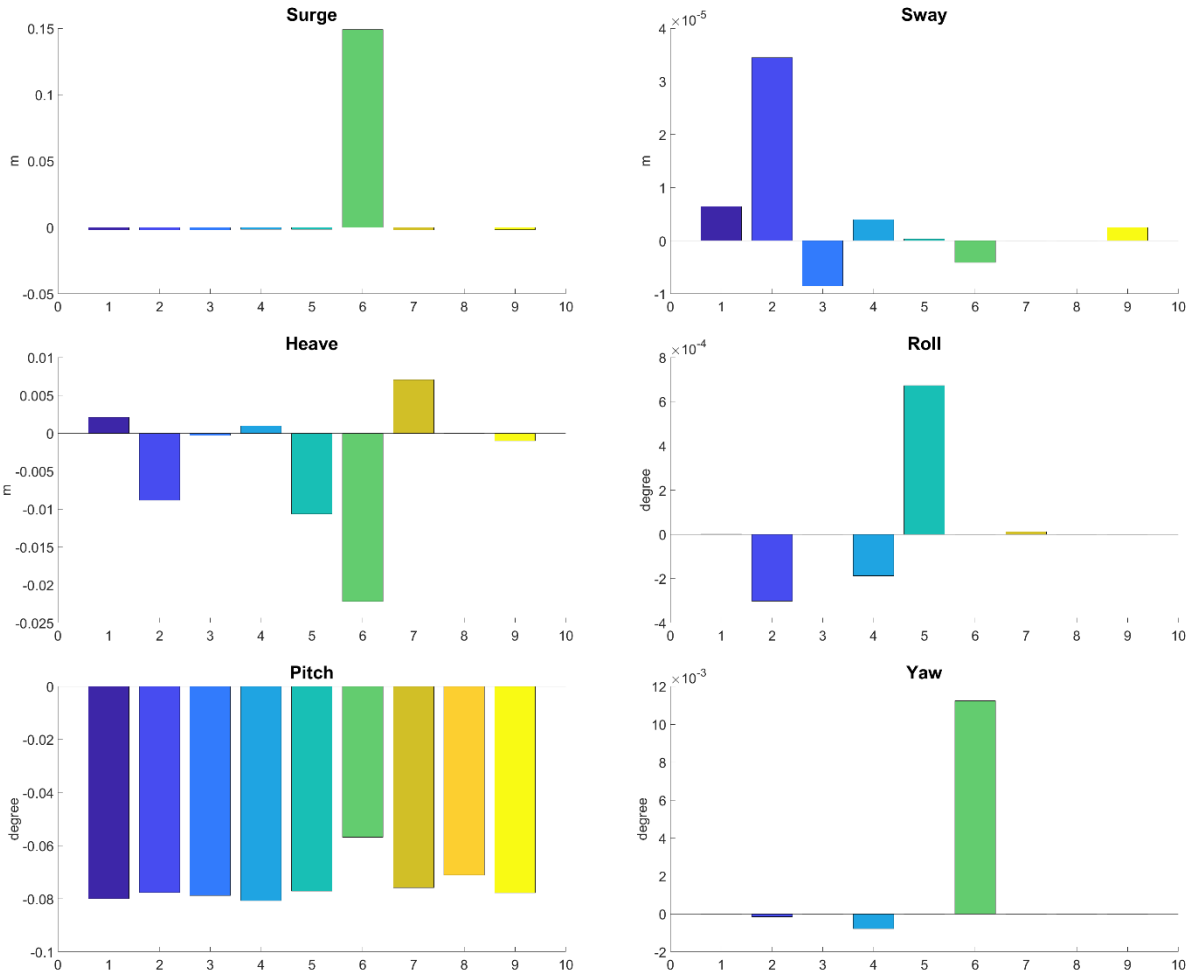

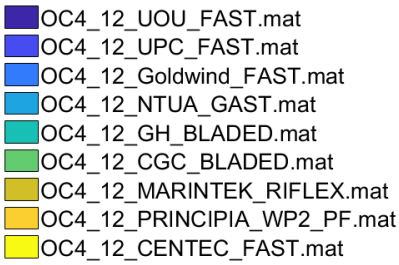

Figure 6: Static equilibrium position of the OC4 System

3.2.2 Free decay tests

Free decay tests measure the response of a system after an initial excitation like a displacement or an impact. They are performed for one degree of freedom at a time and give information about the linear and nonlinear damping and the inertia of the system [28]. The only enabled degrees of freedom are the movements of the platform and the flexibility of the moorings. The tower, nacelle, drivetrain, and rotor are rigid and the break systems engaged. Within the OC4 project they were performed in surge, heave, pitch, and yaw direction. As in the static equilibrium tests, there is no additional excitement present except the initial displacement. Furthermore, aerodynamics influences are not considered, which can be regarded as performing the tests with an air density of zero.

For the surge free decay test, the platform is displaced by 22 meters in positive surge direction. The test duration is 20 minutes. As figure 7 shows, the codes agree well on the surge movement as well as on the coupled responses in heave and pitch. The only exception is the BLADED code used by POSTECH which shows an offset for the heave response and the FAST result from CENTEC for the pitch which underpredicts the damping of the platform. Quasi-static and dynamic modelling of the mooring lines show similar behaviour, although the damping appears to be slightly stronger in MoorDyn's solution. This results in reduced amplitudes in the responses compared to the quasi-static approach.

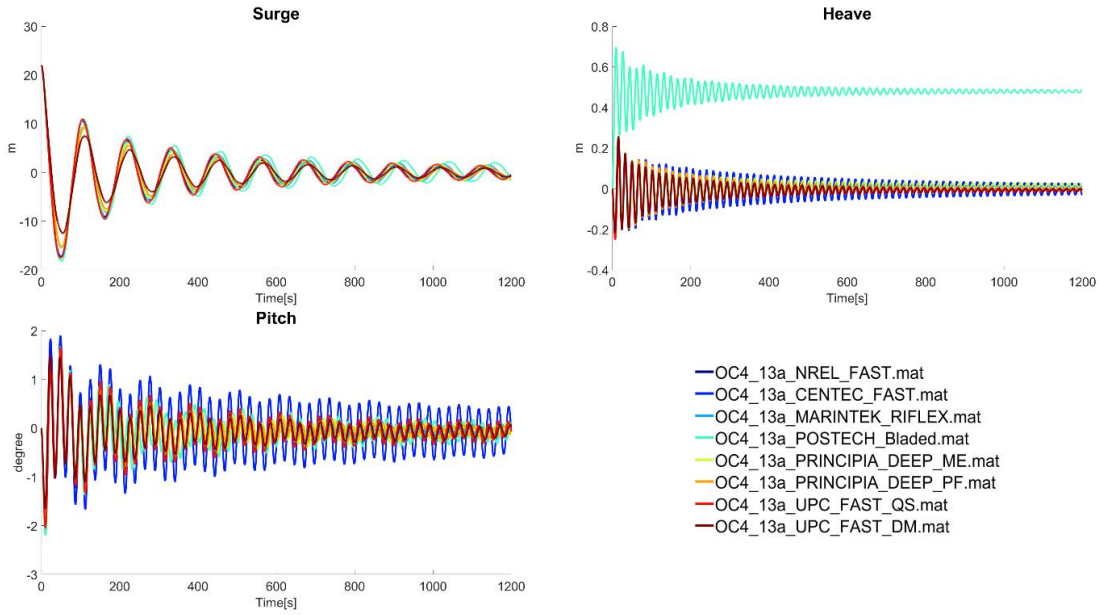

Figure 7: Surge free decay responses of OC4

The heave test is performed by displacing the platform six meter in heave direction. Since the damping in heave direction is significantly bigger than in surge direction, a test time of five minutes is sufficient. The heave response is consistent between the codes, with the DeepLinesWT code used by PRINCIPIA-IFPEN showing a slightly stronger reaction to the displacement in the beginning which quickly aligns with the other codes. This effect is presumably caused by a deviation in the radiation damping coefficient. BLADED displays a marginal offset of the mean value. The coupled pitch movement shows a distinct grouping. The first group which only applies potential flow theory cannot model the coupled pitch damping. Codes utilizing Morrison's equation or Potential Flow enhanced by quadratic drag terms are able to display it. The coupled surge movement agrees in the magnitude of the output, with DeepLinesWT again showing a slightly different behaviour. MoorDyn and MAP++ show nearly no differences in their outputs.

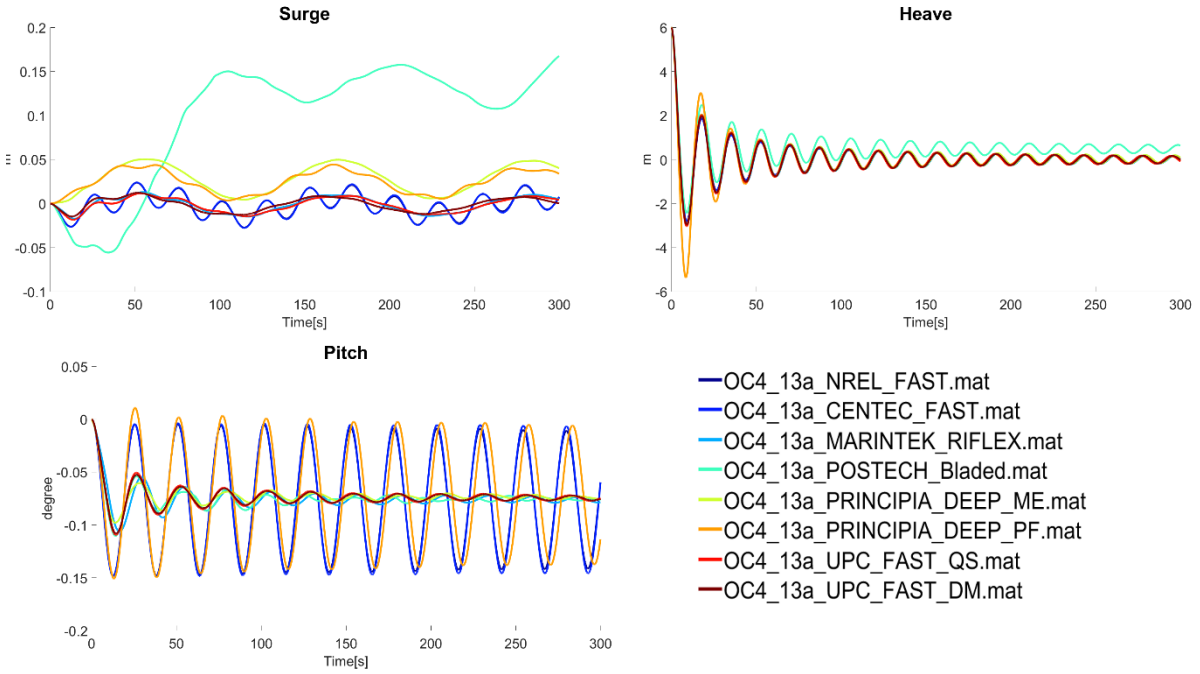

Figure 8: Heave free decay responses of OC4

Figure 9 shows the results for the free decay test in pitch direction. The platform was displaced by eight degrees in positive pitch direction and monitored for five minutes. All participants achieve comparable results for the pitch movement with the FAST model from CENTEC displaying a lower damping value and therefore a higher amplitude. The coupled movements show no characteristic grouping between the codes. Nevertheless, a significantly different behaviour is visible for the BLADED code. Quasi-static and dynamic mooring models deliver, as in the heave free decay, similar results.

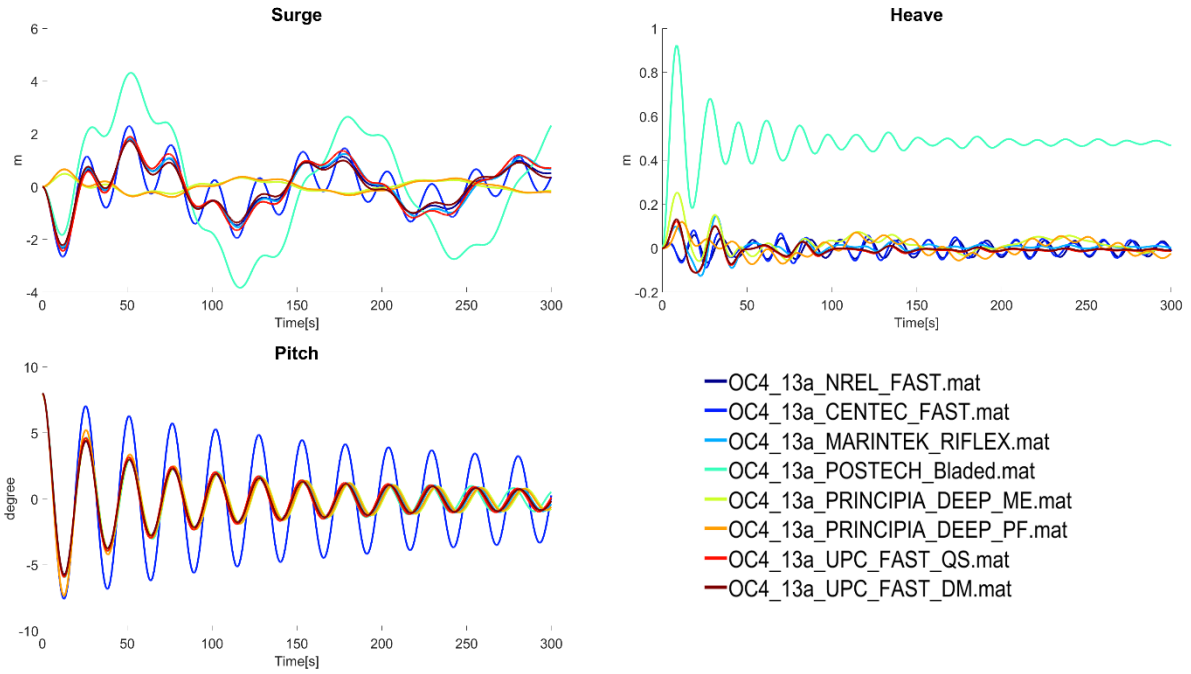

Figure 9: Pitch free decay responses of OC4

As seen in figure 10, the initial yaw displacement is similar to the pitch displacement eight degrees in positive direction. The codes match closely in the yaw and coupled pitch reaction of the platform. The coupled surge motion differs strongly for the BLADED code as well as the potential flow only solution from PRINCIPIA which show significantly longer periods in their response signal.

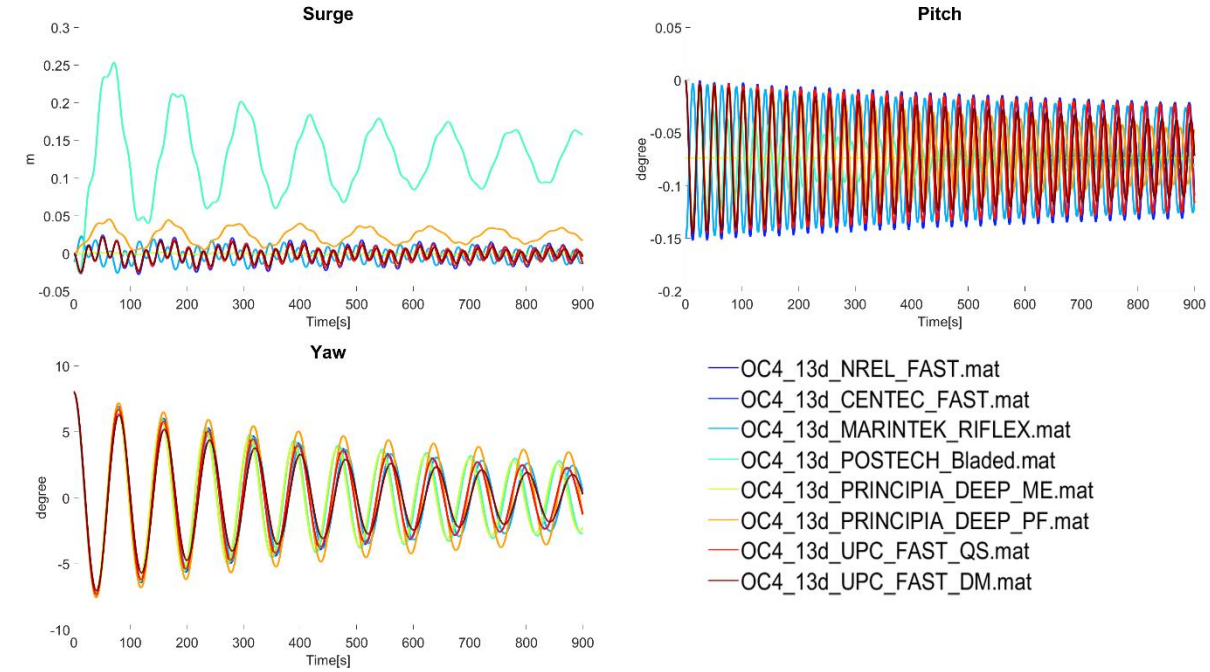

Figure 10: Yaw free decay responses of OC4

Two main contributors to the differences in the free decay responses can be identified. Firstly, the disparity in the modeling of the mooring system (quasi-static or dynamic) and secondly the used hydrodynamic model (potential flow, Morison's equation, or a combination). Inclusion of the mooring

dynamics leads to a slightly increased damping, especially in the surge and yaw tests. Additionally, some of the coupled movements cannot be modeled correctly by hydrodynamic codes disregarding 2nd order effects. The viscous loads have a stronger effect on the overall motion response, whereas the smaller movements are more strongly influenced by radiation damping.

3.2.3 Inverse pendulum tests

Inverse pendulum tests investigate the system's response to excitation solely by waves without any influences of wind. Therefore, the platform, moorings, and tower are modelled as flexible to calculate the platform's response to the hydrodynamic loads. The degrees of freedom for nacelle, drivetrain, generator and rotor are disabled [29]. Two load cases from this test series, an inverse pendulum test with stochastic waves in load case 2.2 and a Response Amplitude Operator (RAO) estimation in load case 2.6, are examined

Load case 2.2: Inverted Pendulum with stochastic waves

Load case 2.2 looks at the response of the platform to an excitation with irregular airy waves. A JONSWAP spectrum with a peak-shape parameter of 2.87 is used to create the waves. They have a significant wave height of six meters and a peak spectral period of ten seconds. The results of the test are presented as mean values of the responses after the transients ceased.

As can be seen in figure 11, the surge response varies greatly between the codes, because some codes account for drift forces in the hydrodynamic calculations and some don't. Codes that only utilise first order potential flow solutions or Morison's equation without wave stretching at the initial position cannot compute those forces and therefore show a zero-surge result. As mentioned in the final report about OC4-Phase II [13], in a realistic scenario a slight drift will occur. It can be captured by taking the second-order terms for potential flow models into account, applying a mean-drift force or applying Morison's equation not only at the mean but also the instantaneous position of the platform. The codes mostly agree on the pitch with the exception of the FAST code from IST which includes second-order difference terms in the potential-flow solution. The model of the UPC used here also shows a lower pitch although second order forces are not considered. The variation of the modelling approach has almost no notable effect on the response. The tower bending moment, which is an important design criterion in offshore wind systems, shows differences of up to 25% between the codes for the mean value. To further understand the significance of these results, the variance of the response must be considered as well.

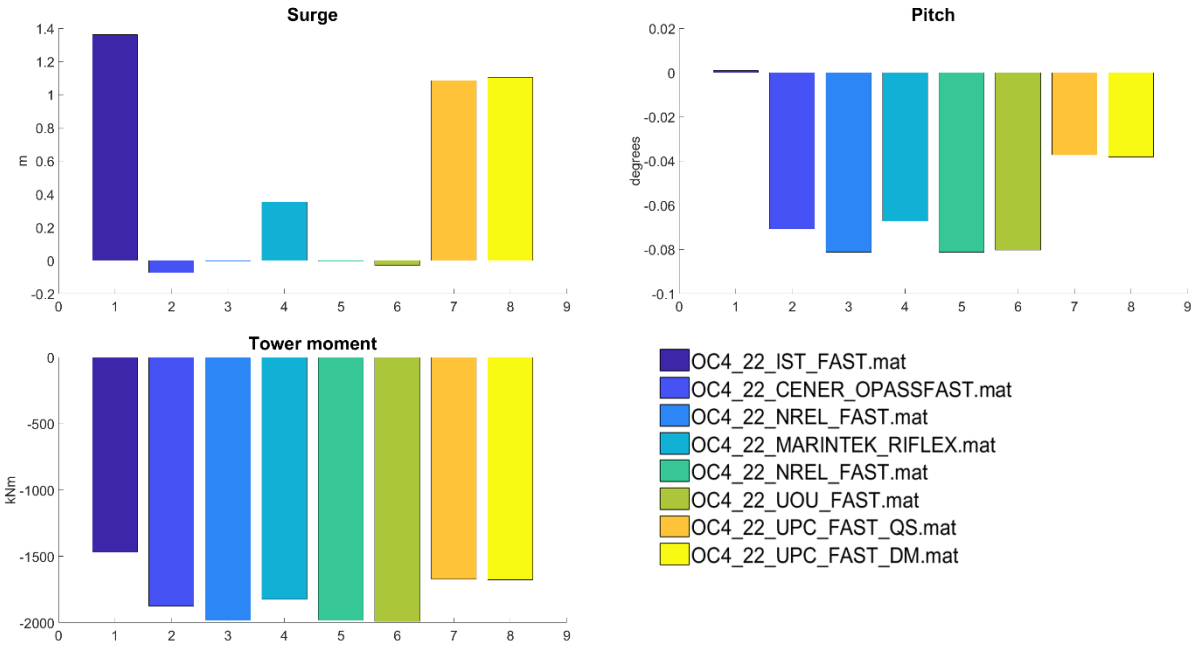

Figure 11: Average responses for load case 2.2

The variance presented in figure 12 is the square of the standard deviation and gives valuable information about how much the response signal deviates from its average value. A high variance can be an indicator for significant fatigue loads. The surge response in particular exhibits a strong disparity between the codes which could be either due to different hydrodynamic calculation models or due to not omitting the transients correctly [30].

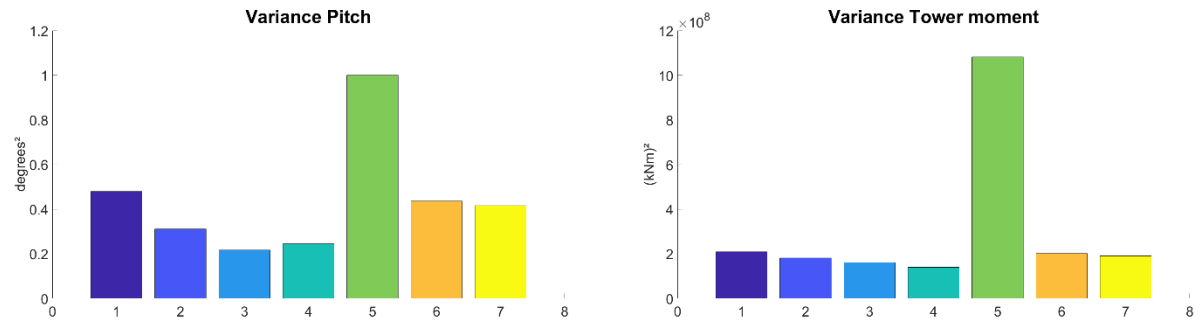

Figure 12: Variance of responses for load case 2.2

Load case 2.6: RAO estimation without wind

Load case 2.6 estimates the Response Amplitude Operators (RAO) for white noise waves with a power spectral density of 1 m^2/Hz during a frequency band from 0.05-0.25 Hz. The RAO is the frequency function of the relationship between wave surface elevation amplitude and the vessel response amplitude. Therefore, it presents the ratio of system response to the wave amplitude. It generally consists of a pair of numbers which signify the amplitude and phase lag between the two. The output of FAST is given as a time series. This time series is converted into the frequency domain with the help of a fast Fourier transform function (FFT) in MATLAB. Afterwards, the RAO is calculated by applying the following formula:

$$RAO = H(\omega) = \frac{S_{xy}(\omega)}{S_{xx}(\omega)} \tag{4}$$

S_{xy} is the cross spectral density of the regarded output variable and the wave surface elevation and S_{xx} the auto spectral density of the surface elevation [31]. Figure 13 shows the frequency responses of the platform. Figure 13 shows the platform's response in the frequency domain. The results are fairly similar between the participants. The heave response shows a clear peak at around 0.058 Hz which coincides with the platform's natural frequency for the heave movement. The natural frequencies for surge and pitch are with 0.01 and 0.04 Hz outside of the wave spectrum as can be seen in their respective power spectral densities. Therefore, the excitation which is visible in the plots of the Response Amplitude Operators must come from other nonlinear sources like higher-order terms of the potential flow solution or nonlinear wave loads from Morison's equation. The exception is the HYDRO-GAST code from NTUA that uses Morison's equation for its hydrodynamic modelling. It shows a significantly higher peak for the heave movement as well as a different behaviour in the pitch response than the other codes. Furthermore, the GH BLADED code shows a similar trend in pitch as the other codes but with a greater displacement.

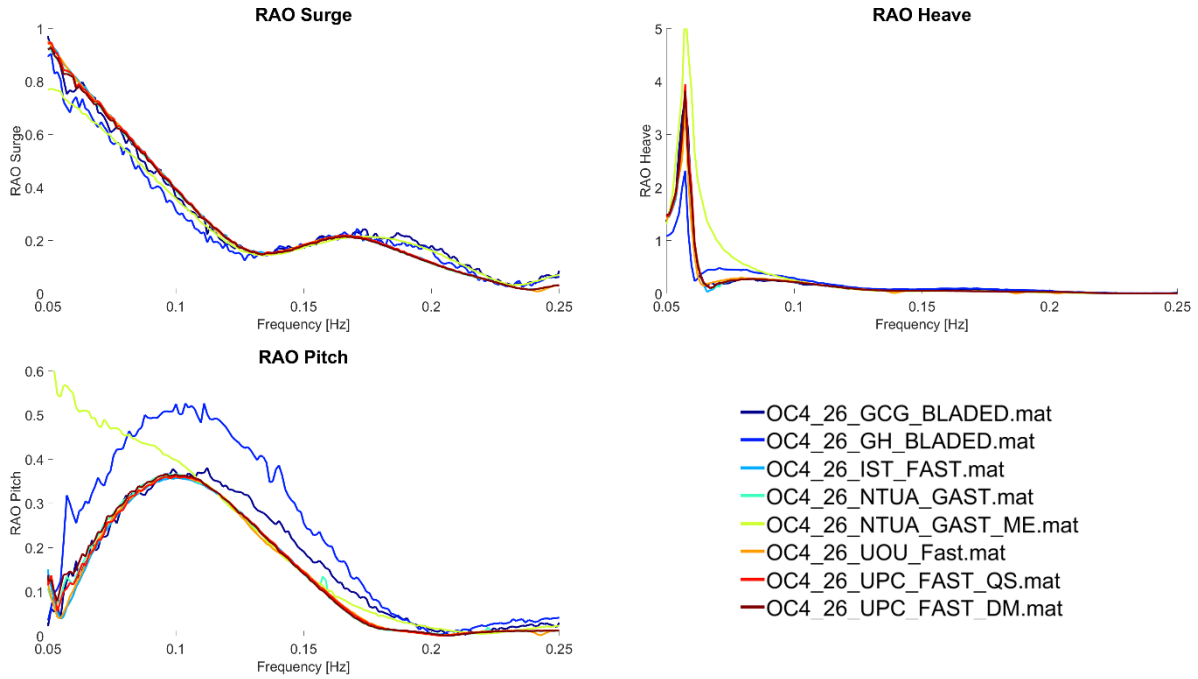

Figure 13: Response Amplitude Operators of the OC4 platform without wind excitation

The RAO of the tower moment in fore/aft direction shows no significant peak due to the natural frequency of the tower being outside of the frequency spectrum of the wind at 0.43 Hz. The codes agree well on the RAO with the exception of GAST with Morison's equation in the low frequency area and a general overprediction of the response by the BLADED code. The mooring system shows a distinct grouping of those codes, that take into account the dynamic loads and those, that only utilise a quasi-static mooring. Codes which disregard these terms heavily underpredict the loads in the range above 0.13 Hz. The difference in the mooring models is also visible in the FAST version used in this thesis. Since fatigue loads

can have a significant influence on the lifetime and stability of the mooring system it seems necessary to apply dynamic modelling approaches.

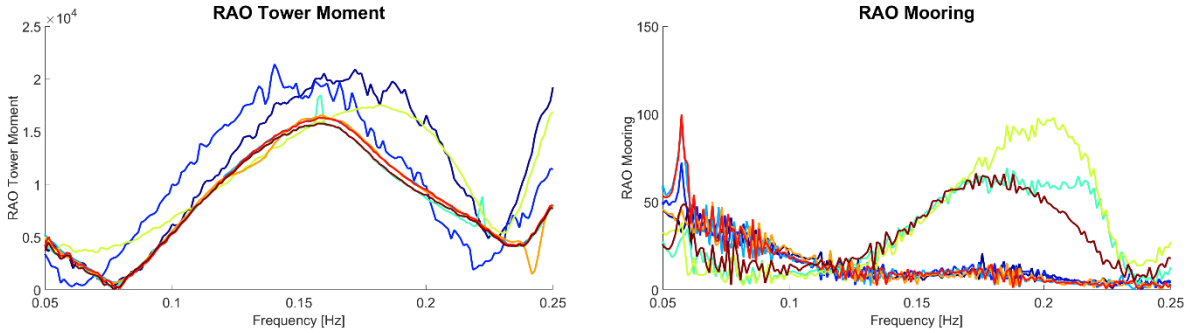

Figure 14: Response Amplitude Operators for the tower and mooring system

3.2.4 Full-system analysis

The last section of tests are full-system analyses. They feature simultaneous wind and wave excitation on a completely enabled turbine system. Different load cases (3.2, 3.4 and3.7 from the initial project) are considered ranging from regular wind and waves to stochastic scenarios and a sea current induced load.

Load case 3.2: Stochastic wind & wave excitation

In load case 3.2 the turbine starts the analysis running at its rated speed of 12 rpm. The same irregular airy wave excitation as in load case 2.2 is used with a significant wave height of six meters and a wave period of ten seconds. The JONSWAP spectrum again has a peak-shape parameter of 2.87. The wind is a stochastic wind field with a mean wind speed at the hub height of 11.4 m/s. It is modelled with Mann's turbulence model with a shear factor of 0.14.

Figure 15 shows the mean values of response for surge, pitch, and the tower moment. Compared to load case 2.2, which features the same wave excitation without wind a reduction of the differences in the codes is observed. This is due to the thrust force applied by the wind which is significantly higher than the mean drift forces. This also leads to greatly increased loads and offsets on the platform.

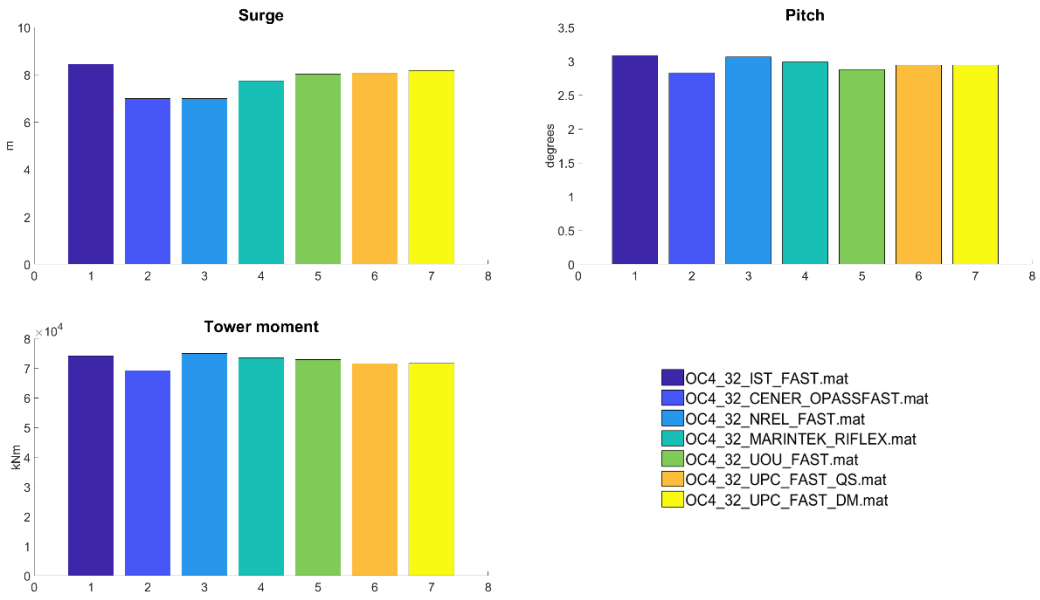

Figure 15: Average responses for load case 3.2

Compared to load case 2.2, the variance is larger in the case with wind excitation. This effect is especially pronounced in the surge direction, but affects all other measured values as well. Again. the reasons for these high variances of response in some codes could be a failed attempt of removing the transients properly or by differences in the aerodynamic models.

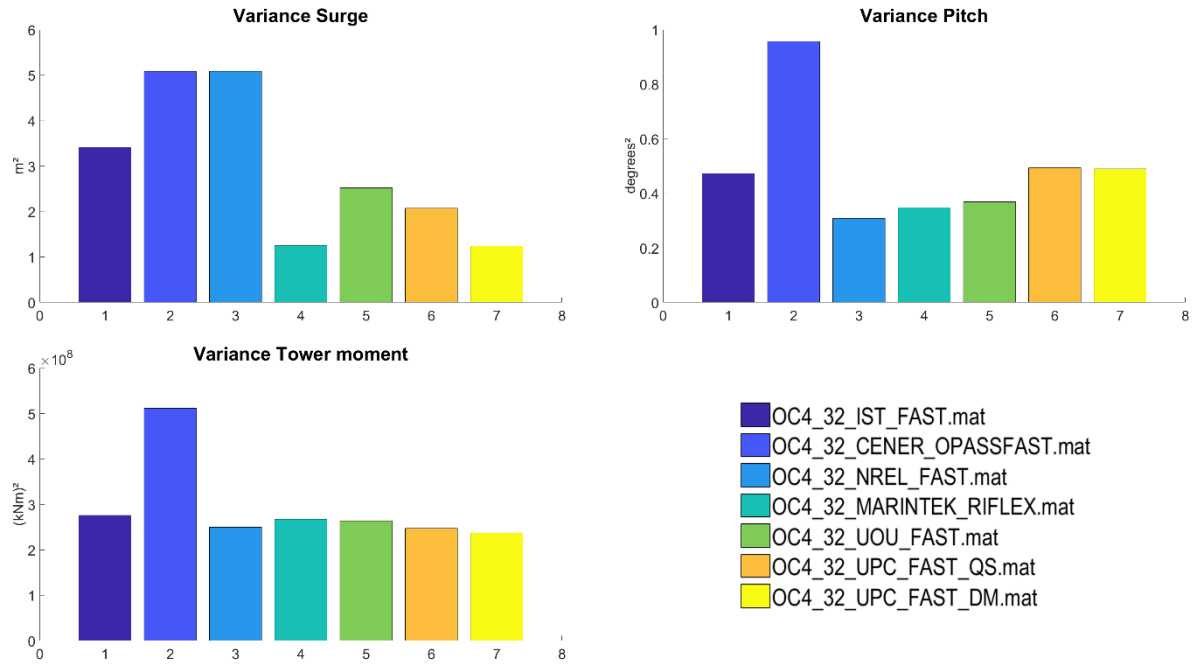

Figure 16: Variance of responses for load case 3.2

Load case 3.4: ´Steady Wind & Current

Load case 3.4 introduces a current to the analysis. It has a mean surface speed of 0.5 m/s which is decreasing with the water depth according to the following power law relation:

$$U(z) = U_{surface} \cdot \left(\frac{z+d}{d}\right)^{\frac{1}{7}} \tag{5}$$

Z is the water depth in which the current speed is regarded and d the maximum water depth at the platform location. In addition to the current the test features regular Airy waves with a wave height of six m and ten seconds period. Furthermore, the turbine is excited by a steady and uniform wind inflow without shear and a mean wind speed of 8 m/s.

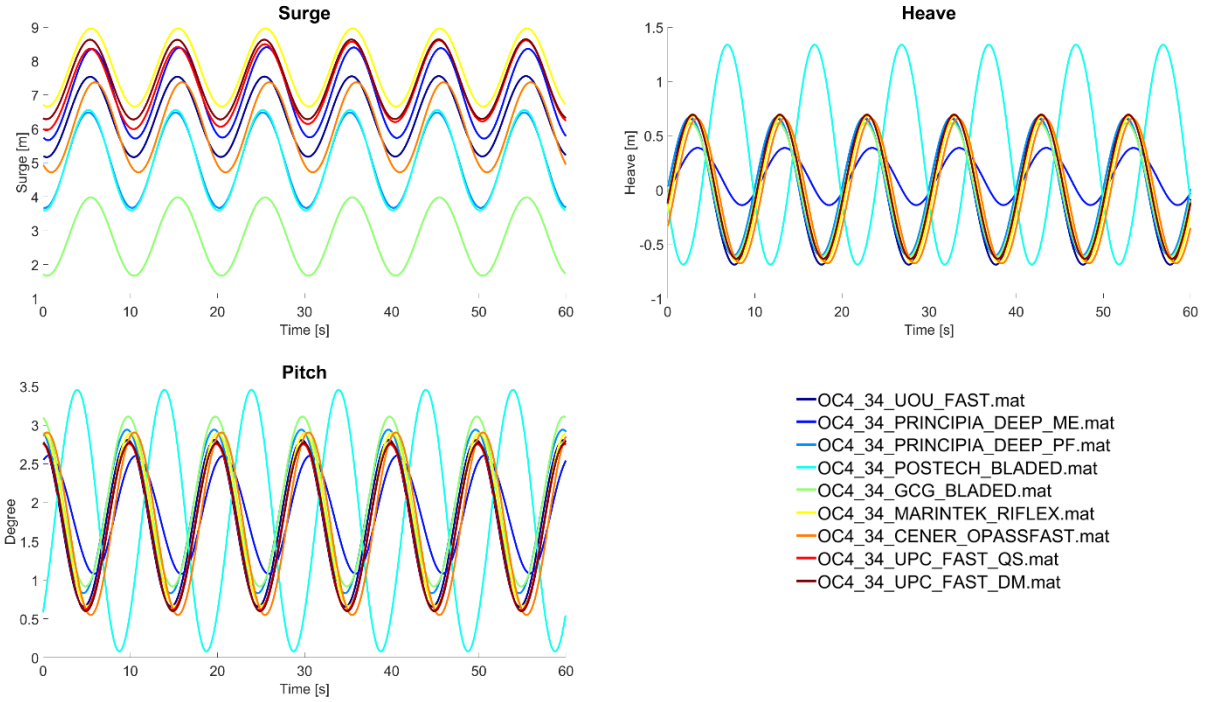

Figure 17: Surge, heave, and pitch response for load case 3.4

The mean value of the surge responses varies significantly between the codes depending if second order terms for the potential flow theory or wave stretching at the instantaneous platform position for Morison's equation is considered. The heave and pitch responses for most codes agrees fairly well, with the exception of the BLADED code from POSTECH, which overpredicts the amplitude due to too little damping and the Morison's equation solution from PRINCIPIA which utilises too much damping. The use of dynamic or quasi-static mooring approaches has only a very small effect on the platform's response for this load case.

Load case 3.7: RAO with wind

The last test performed for the OC4 project is the investigation of the influence of wind on the Response Amplitude Operators (RAO). The initial conditions are identical to those from load case 2.6, except for the introduction of a steady and uniform wind with a mean wind speed of 8 m/s. Figure 18 shows the small influence the wind excitation has on the RAO of the platform movements. The responses for surge, heave and pitch show the same behaviour as without wind in load case 2.6. This behaviour is expected due to the dominance of the linear wave loads in the examined frequency spectrum which are sufficiently captured by all codes. The only exception is the BLADED from GH, which varies significantly from the other codes for all movements. Furthermore, the pitch movement in the GAST version that utilises Morison's equation differs heavily from other codes especially in lower frequencies.

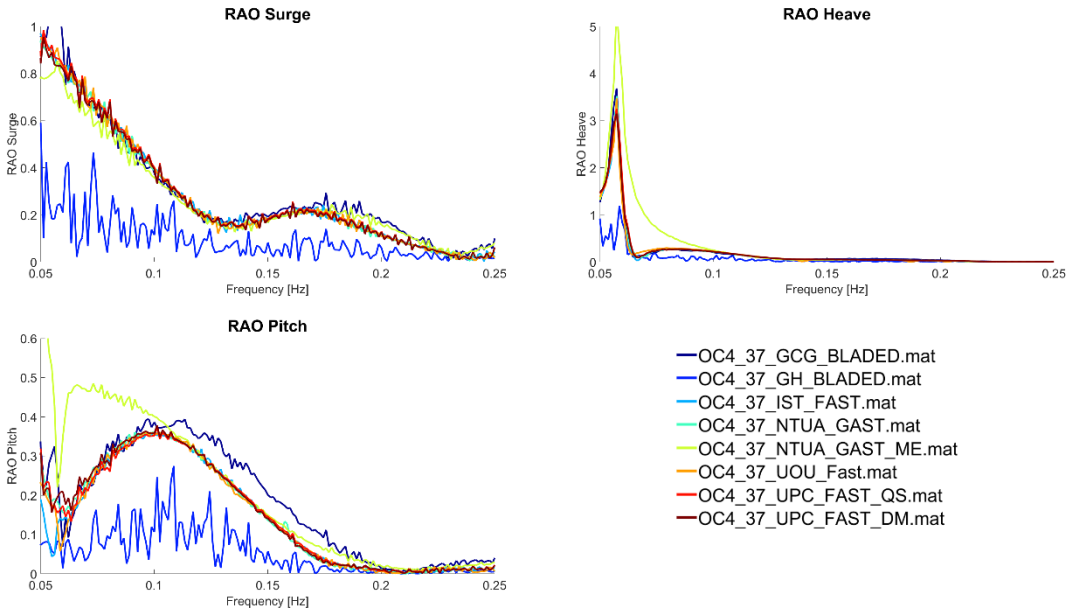

Figure 18: Response Amplitude Operators of the OC4 platform with wind excitation

As in the test without wind inflow, the codes mostly agree on the response with the exception of BLADED from GCG which slightly overpredicts it. The GH output shows the same irregularity as in the RAOs for surge, heave, and pitch. The mooring loads increase the most significantly with the wind, especially in the region above 0.13 Hz which is only captured by codes with a dynamic modelling approach. The same grouping as in load case 2.6 is visible. The newer FAST version matches earlier codes if a quasi-static mooring model is used. If MoorDyn is utilised, the results resemble other codes which consider dynamic loads.

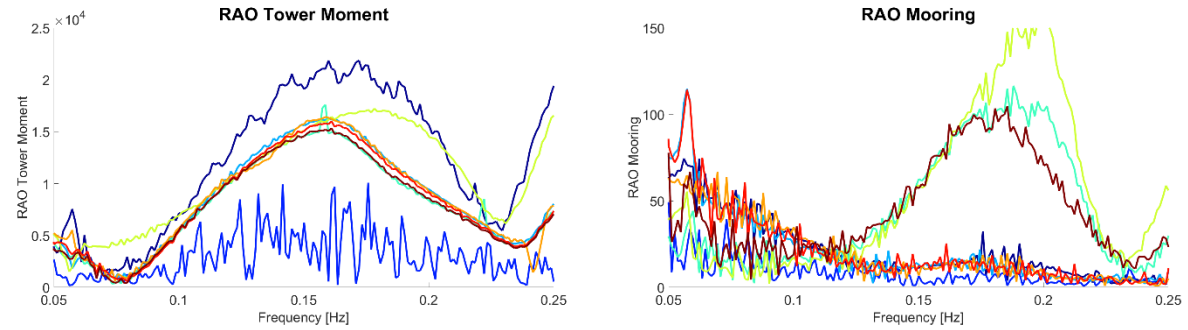

Figure 19: Response Amplitude Operators for the tower and mooring system

3.3 Summary

The OC4 Code Comparison Collaboration proved a useful project to evaluate the differences and problems of a wide variety of offshore codes and modelling approaches. It allows a deeper understanding of the complex dynamic behaviour of floating offshore system in combination with wind and wave excitation. Thus, it provides valuable information about the strengths, weaknesses, and limitation of hydrodynamic, aerodynamic, and mooring system models within a wide spectrum of external conditions. In accordance with the findings of the initial OC4 project several conclusions can be drawn [13]:

The semisubmersible platform of OC4 can be sufficiently described by codes that use either potential flow or Morison's equation. The potential flow codes deliver adequate results even if radiation and diffraction loads are not considered. In severe conditions, the approximation of viscous loads by adding a global drag matrix to the PF solution is not exact enough compared to adding specific drag terms from ME. To correctly model drift forces second order terms or a mean drift force have to be implemented, in particular in cases without wind excitation.

The codes based on Morison's equation display a larger fluctuation especially in the pitch responses which might be an issue leading to fatigue problems. To achieve a realistic assessment of drift forces in ME, it is necessary to consider the instantaneous position of the platform and apply wave stretching. Additionally, due to the shallow draft of the semisubmersible platform, ME models need to take the dynamic pressure on the base columns into account to capture the correct heave response during wave excitation.

The mooring loads can be calculated with quasi-static or dynamic codes which will both assess the extreme loads well enough. This thesis uses both models while keeping the other input parameters constant to obtain detailed information of the differences. In general, the choice of the calculation model has no significant impact on the prediction of the platform movements. In lower frequencies, the mooring loads also agree within both models. The gravest differences occur in higher frequencies, where a distinct underprediction of the mooring loads in the lines are observed in quasi-static models. While this has only limited impact on the whole system dynamic, it might lead to fatigue damage in the mooring lines and needs to be inspected closely. A dynamic modelling seems, especially for cases with strong wind excitation, necessary.

Response Amplitude Operators prove to be a reliable indicator for the characteristic of the response of the system to various wave and wind conditions and are very similar in all compared codes.

FAST V8.16 is able to simulate all load cases and produces results comparable to the initial study. Moreover, it shows no big disparities or deviations.

OC4 will be a valuable support and guideline for the development of future design and analysis tools for offshore wind turbines. Nevertheless, it only provides a comparison and benchmark of the investigated codes which does not allow to draw reliable conclusions about the accuracy of the codes compared to the real behaviour of the system. This will be addressed by the OC5 project in the following chapter, which compares offshore codes with measurements from experiments conducted on a scaled model of a turbine.

4 OC5 Phase IIb – Semisubmersible Platform

4.1 Overview

Code-to-code comparison, as performed in previous projects, cannot correlate the accuracy of their results to real behaviour. Therefore, to validate the theoretical results from OC4 and to see how they compare to experimental values the Offshore Code Comparison Collaboration is continued with the OC5 project. It stands for *Offshore Code Comparison Collaboration, Continued, with Correlation* and is led by the International Energy Agency (IEA). As the OC4 project, it features a wide range of participating institutions, codes, and modelling approaches. Further details about the participants and used codes can be found in chapter 4.1.3. The project is divided into two phases: [32]

Phase I analyses the hydrodynamic loads on a fixed cylinder during wave excitation. This simplistic experiment gives detailed information about the maturity of the used hydrodynamic codes due to the minimalization of influencing factors. It also shows the limitations and capabilities of the different software tools to correctly predict the loads before moving on to more complex and extensive tests and structures. Furthermore, this phase is also used to establish the methods for the model calibration and validation. The experiments are conducted in the wave tank of MARINTEK in the Netherlands as well as in Denmark by the Technical University of Denmark (DTU) and the Danish Hydraulic Institute (DHI). It involves tests under regular und irregular wave conditions to obtain the hydrodynamic coefficients and to examine the importance of using higher-order approaches in the codes. In phase I-a several rigid steal cylinders with varying diameter are fixed in a framework according to figure 20 and subjected to waves.

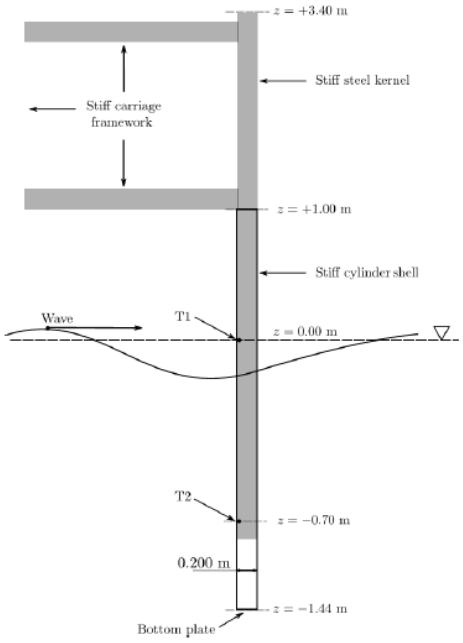

Figure 20: OC5 - Phase I Setup

Phase I-b repeats these experiments with a flexible cylinder fixed on a sloped seabed to obtain parameters for seabed models. In the first step, the model and wave parameters are calibrated by approximating

hydraulics coefficients and wave height and period. Then twelve load cases with regular and four with irregular waves are performed. They findings of phase I show a need for the inclusion of higher-order terms in the hydrodynamic calculations to capture the nonlinear behavior in the model [33].

Phase II takes the experiments further and uses a performance-scaled model of the NREL 5MW turbine called the MARIN Stock Wind Turbine (MSWT) mounted on top of the OC4 semisubmersible platform. Details about the model, the modifications on the turbine and platform compared to the OC4 project can be found in the following chapters. It assesses the ultimate and fatigue loads on a 1:50 scaled turbine model and compares them to the theoretical results obtained by various offshore design codes. The model was built and tested in the MARIN offshore basin in the Netherlands by the DeepCWind consortium in 2013 [32].

This thesis focuses on phase II of the OC5 project. It aims to show the occurring differences between calculating the hydrodynamics with Potential Flow and a model based on Morison's equation. First, the input files for the changed system are established in FAST. Afterwards a variety of load cases are run and the test results are compared with the experimental findings and the outputs of the other participants.

4.1.1 Experimental setup and scaling

OC5 utilises model testing to gain empirical data for a comparison with various offshore codes. For this reason, a 1:50 scaled model is built and tested under various conditions in the wave tank of the Maritime Research Institute Netherlands (MARIN). The tank has a diameter of 45 x 36 meter with a depth of 20 meter at the deepest point [34]. The loads and displacements of the turbine are measured by a variety of sensors. The cables to these sensors are bundled and lead from the middle of the tower to the computers. This cable bundle and also the sensors on the system add additional weight, stiffness and preload to the system which has to be accounted for in the codes.

The wind excitation is realised by an array of 35 fans with alternating direction of rotation clustered in five rows of seven fans each. The wind flow is straightened after every fan and run through two honeycomb screens with a nozzle in between. The system is located above the SWL to keep interaction with the waves to a minimum and tilted down by 2.5 degree to align the most homogenous part of the flow with the area swept by the rotor blades. These measures lead to a homogenous elliptical flow field with negligible swirl and only around 5% turbulences for the rotor area (represented as the circle) as shown in figure 21 [35]:

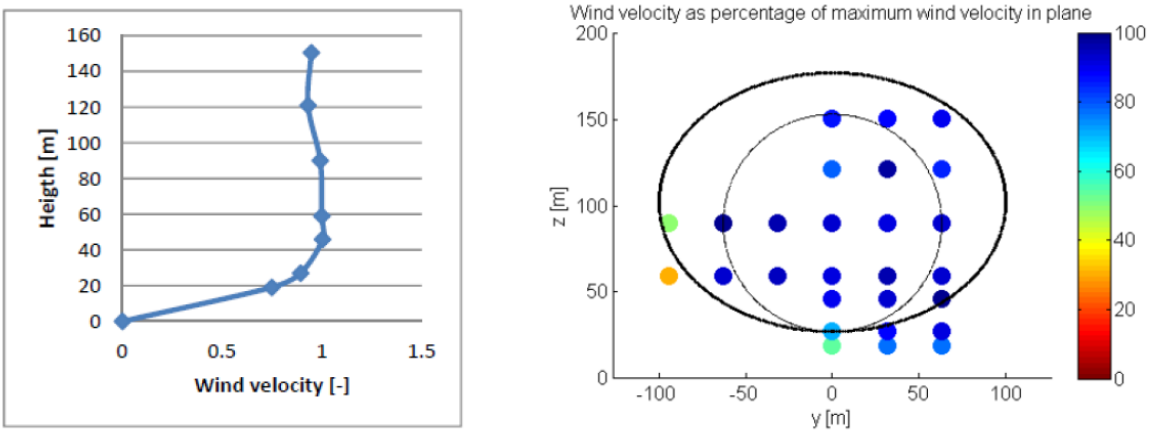

Figure 21: Averaged vertical wind velocity and wind field velocity in the rotor plane [35]

The waves are produced by flap-type wave makers with separate motors for each of the 40-cm wide, hinged flaps. They can create various wave types from different angles of attack, although OC5 uses only waves from an angle of 180°, which means that they hit the turbine straight from the front [34].

Both wind and waves are upscaled with the same scaling method as the turbine and the occurring loads. In order to not only ensure geometrical but also kinematic and dynamic similarity a method called Froude scaling is used. It is a proven method for offshore structures which relies on keeping the Froude number equal between model and prototype. The Froude number is thereby defined as the ratio between inertia to gravity forces:

$$Fr = \frac{u^2}{gD} \tag{6}$$

and therefore

$$Fr_{Prototype} = Fr_{Model} \tag{7}$$

Assuming equal water density, it utilises only one geometric scaling factor $\lambda = \frac{1}{50}$ to derive all relevant parameters for the model. A list of which parameters is influenced in which way by the scaling factor is displayed in table 4 [36].

Table 4: Scaling parameters for Froude scaling

Parameter	Unit	Scaling factor
Length	[m]	λ
Time	[s]	$\sqrt{\lambda}$
Mass	[kg]	λ^3
Force	[N]	λ^3
Moment	[Nm]	λ^4
Acceleration	[m/s²]	1

Pressure	[N/m²]	λ
Inertia	[m²kg]	λ^5

A major drawback of this scaling method is that the Reynolds number of model and prototype do not agree if Froude scaling is applied, due to the difference in their scaling coefficients. The Reynolds number is the ratio between inertia and viscous forces and describes the flow conditions.

$$Re = \frac{\rho D u}{\mu} \tag{8}$$

which leads together with the scaling factors of table 4 to:

$$Re_{Prototype} = \lambda^{3/2} \cdot Re_{Model} \tag{9}$$

As can be seen, the Reynolds number for the full-scale prototype is bigger than for the model. Thus, a laminar flow at model scale can turn into a turbulent flow at full-scale, which introduces new physical effects and deviations to the experimental results [36]. This was addressed in the experiment by adjusting the turbine, in particular the blades, in a way that the resulting thrust force and torque matches the real behavior. These modifications allow a proper upscaling of the turbine model and are explained in more details in the following chapter. All values presented in this thesis are upscaled to the prototype to allow comparison with previous studies [37].

4.1.2 Differences to OC4 model

As mentioned in chapter 4.1.1, the main differences between model/prototype used in OC5 compared to OC4 are in the design of the turbine blades. The utilised Froude scaling leads to a deviation in the Reynolds number between model and prototype. Thus, the occurring thrust and torque loads will differ greatly in the wind environment of the experiment where low Reynolds numbers are to be expected [32].

To accommodate this change and make sure that the results scale properly, a new turbine is develop called MARIN Stock Wind Turbine (MSWT). The chord of the turbine blades is thicker than in the NREL 5 MW turbine and only two different airfoil shapes, a cylindrical and the AG04 foil, are used. Furthermore, the structural parameters from the rotor-nacelle-assembly and the tower are changed together with the ballast distribution of the platform to achieve the correct center of mass for the system. The properties of the full system are listed in table 5:

Table 5: OC4 full system parameters

Parameter	**Value**
Mass	1.3958E+7 kg
Draft	20 m
Displacement	1.3917E+4 m^3
CM location below SWL	8.07 m
Roll inertia about system CM	1.3947E+10 kgm^2

Pitch inertia about system CM	1.5552E+10 kgm^2
Yaw inertia about system CM	1.3692E+10 kgm^2

Further details about the system are available in the NREL reports regarding the definition of the OC5 DeepCWind semisubmersible floating system [35].

4.1.3 Participants and used codes

Table 6 shows the participants and the codes they use for the calculation of the aerodynamics, hydrodynamics, and the mooring system. A wide variety of models is employed, especially in the field of hydrodynamics. Most codes use either Morison's equation, a Potential Flow solution (1st or 2nd order) or a combination of both. To capture viscous effects, some of the potential flow models are enhanced with either a damping matrix (indicated as pink square under 1st PF) or the drag term from Morison's equation (green squares under ME, 1st PF or 2nd PF). Participants only utilising Strip Theory are marked with a pink square under ME. Furthermore, some codes work with wave stretching for the wave kinetics (stretch), use the instantaneous platform position to calculate wave loads (inst. Pos.) or the measured wave instead of a synthetic wave with JONSWAP spectrum.

The aerodynamics are solved by most codes with a blade-element momentum (BEM) theory-based model. It is augmented by most participants with the inclusion of a dynamic wake and the influence of unsteady airfoil aerodynamics. This allows the calculation of effects like flow hysteresis, including unsteady attached flow, trailing-edge flow separation, dynamic stall, and flow reattachment.

The mooring loads are either assessed with a quasi-static or dynamic approach which are complimented by hydrodynamic wave excitation on the mooring lines and the friction between the lines of the catenary system and the seabed.

The acronyms of the table 6, which gives an overview of the used codes, have the following meaning[32]:

Aerodynamics
- Dyn. Wake = Dynamic Wake
- Unst. Airfoil = Unsteady airfoil Aerodynamics

Hydrodynamics
- 2nd+ WK = Second-order (or higher) Wave Kinematics
- 1st PF = First-order Potential Flow model (green = Morison drag also included via strip theory, pink = viscous drag approximated by a damping matrix)
- 2nd PF = Second-order Potential Flow model
- ME = Morison Equation (pink = full, green = only drag term)
- Meas. Wave = Measured Wave elevation
- Stretch = Wave Stretching
- Inst. Pos. = Hydrodynamic forces calculated at the Instantaneous Position of the structure

Moorings
- Dyn. = Dynamic mooring model
- Hydro Exc. = Hydrodynamic loads on the moorings due to wave Excitation
- Seabed Fric. = Seabed Friction

Table 6: Participants and used codes in OC5

Participant	Code	Aerodyn.		Hydrodynamics							Moorings		
		Dyn. Wake	Unst. Airfoil	2nd + WK	1st PF	2nd PF	ME	Meas. Wave	Stretch	Inst. Pos.	Dyn.	Hydro Exc.	Seabed Fric.
4Subsea	OrcaFlex-FAST v8												
CENER	FAST v6 + OPASS												
CENTEC	FAST v8												
DNV GL	Bladed 4.8												
DTU ME	HAWC2												
DTU PF	HAWC2												
ECN-MARIN	aNySIM-PHATAS v10												
IFE	3DFloat												
IFP_PRI	DeepLines Wind V5R2												
NREL PF	FAST v8												
NREL ME	FAST v8												
POLIMI	FAST v8.15			Diff.-only									
Siemens PLM	Samcef Wind Turbine												
Tecnalia F7O	FAST v7 + OrcaFlex 9.7												
Tecnalia F8	FAST v8.16												
UC-IHC	Sesam												
UOU	UOU + FAST v8												
UPC	UPC + FAST												
UTokyo	NK-UTWind												
WavEC FAST	FAST v8												
WavEC FF2W	FF2W												

Both the PF and the ME model used in this chapter utilise FAST version 8.16 with dynamic mooring calculations.

4.2 Analysis

4.2.1 The OC5 model in FAST

The first step to comparing the experimental results with the codes is to establish sophisticated models of the system in the input files of FAST 8.16. The files for the OC4 models are changed according to the modifications mentioned in the previous chapters. The HydroDyn input file is adjusted by adding an additional preload in surge to model the influence of a cable bundle which effectively acts as a fourth mooring line. A problem that occurred during the creation of the model is the lack of information about the weight and ballast distribution in the turbine. In contrast to the OC4 model, only the total mass of the system including ballast is known. An approach to fix this problem is to model the ballast as part of the platform instead of using waterfilled columns.

4.2.1.1 Potential Flow model

FAST coupled with WAMIT and HydroDyn accounts for the mass of the filled members in the additional linear damping matrix of the HydroDyn input file while WAMIT takes care of the buoyancy restoring Thus, as figure 22 shows, the additional linear damping matrix is zero for all members and the filled member section of the HydroDyn input file is set to “no filled members”. This leads to a heave offset which is counteracted by also adding also a pretension in negative heave direction to achieve a similar draft as the model. The periods in the free decay test agree well with the experimental results, therefore the stiffness, damping, and drag matrixes are left empty.

```
---------------------- PLATFORM ADDITIONAL STIFFNESS AND DAMPING --------------
        98400         0            -5850000      0            0            0   AddF0    - Additional preload (N, N-m)
        0             0            0             0            0            0   AddCLin  - Additional linear stiffness (N/m, N/rad, N-m/m, N-m/rad)
        0             0            0             0            0            0
        0             0            0             0            0            0
        0             0            0             0            0            0
        0             0            0             0            0            0
        0             0            0             0            0            0
        0             0            0             0            0            0   AddBLin  - Additional linear damping(N/(m/s), N/(rad/s), N-m/(m/s), N-m/(rad/s))
        0             0            0             0            0            0
        0             0            0             0            0            0
        0             0            0             0            0            0
        0             0            0             0            0            0
        0             0            0             0            0            0
        0             0            0             0            0            0   AddBQuad - Additional quadratic drag(N/(m/s)^2, N/(rad/s)^2, N-m(m/s)^2, N-m/(rad/s)^2)
        0             0            0             0            0            0
        0             0            0             0            0            0
        0             0            0             0            0            0
        0             0            0             0            0            0
        0             0            0             0            0            0
        0             0            0             0            0            0
```

Figure 22: OC5 HydroDyn with Potential Flow

The ElastoDyn is mostly modified according to the information handed out to the participants and incorporates the changes to the turbine. The new MARIN Stock Wind Turbine has no precone, a bigger overhang of the turbine blades, some small changes in the CM positions and a slightly higher system mass. Details about the exact mass distribution of the tower are unavailable, therefore it is approximated by considering an equally distributed mass along the tower height. The coefficients for the equations of the tower’s bending modes are calculated using a simplified tower model in the Autodesk ROBOT. The masses of rotor, nacelle etc. are implemented as nodal forces in their respective centers of mass. Then a modal analysis is performed, resulting in the coefficients for the first and second fore/aft and side/side bending modes. Figure 23 shows an excerpt of the ElastoDyn file used by both models.

```
---------------------- TURBINE CONFIGURATION ---------------------------------
         3   NumBl       - Number of blades (-)
        63   TipRad      - The distance from the rotor apex to the blade tip (meters)
       1.5   HubRad      - The distance from the rotor apex to the blade root (meters)
         0   PreCone(1)  - Blade 1 cone angle (degrees)
         0   PreCone(2)  - Blade 2 cone angle (degrees)
         0   PreCone(3)  - Blade 3 cone angle (degrees) [unused for 2 blades]
         0   HubCM       - Distance from rotor apex to hub mass [positive downwind] (meters)
         0   UndSling    - Undersling length [distance from teeter pin to the rotor apex] (meters) [unused for 3 blades]
         0   Delta3      - Delta-3 angle for teetering rotors (degrees) [unused for 3 blades]
         0   AzimB1Up    - Azimuth value to use for I/O when blade 1 points up (degrees)
     -10.6   OverHang    - Distance from yaw axis to rotor apex [3 blades] or teeter pin [2 blades] (meters)
     1.912   ShftGagL    - Distance from rotor apex [3 blades] or teeter pin [2 blades] to shaft strain gages [positive for upwind rotors] (meters)
         0   ShftTilt    - Rotor shaft tilt angle (degrees)
      1.13    NacCMxn    - Downwind distance from the tower-top to the nacelle CM (meters)
         0   NacCMyn     - Lateral  distance from the tower-top to the nacelle CM (meters)
         0   NacCMzn     - Vertical distance from the tower-top to the nacelle CM (meters)
   -3.09528   NcIMUxn     - Downwind distance from the tower-top to the nacelle IMU (meters)
         0   NcIMUyn     - Lateral  distance from the tower-top to the nacelle IMU (meters)
    2.23336   NcIMUzn     - Vertical distance from the tower-top to the nacelle IMU (meters)
        1.8   Twr2Shft    - Vertical distance from the tower-top to the rotor shaft (meters)
       88.2   TowerHt     - Height of tower above ground level [onshore] or MSL [offshore] (meters)
         10   TowerBsHt   - Height of tower base above ground level [onshore] or MSL [offshore] (meters)
         0   PtfmCMxt    - Downwind distance from the ground level [onshore] or MSL [offshore] to the platform CM (meters)
         0   PtfmCMyt    - Lateral distance from the ground level [onshore] or MSL [offshore] to the platform CM (meters)
    -14.09  PtfmCMzt    - Vertical distance from the ground level [onshore] or MSL [offshore] to the platform CM (meters)
         0   PtfmRefzt   - Vertical distance from the ground level [onshore] or MSL [offshore] to the platform reference point (meters)
---------------------- MASS AND INERTIA --------------------------------------
         0   TipMass(1)  - Tip-brake mass, blade 1 (kg)
         0   TipMass(2)  - Tip-brake mass, blade 2 (kg)
         0   TipMass(3)  - Tip-brake mass, blade 3 (kg) [unused for 2 blades]
         0   HubMass     - Hub mass (kg)
    115926   HubIner     - Hub inertia about rotor axis [3 blades] or teeter axis [2 blades] (kg m^2)
   534.116   GenIner     - Generator inertia about HSS (kg m^2)
4.779E+05 kg  NacMass     - Nacelle mass (kg)
2.60789E+06   NacYIner    - Nacelle inertia about yaw axis (kg m^2)
         0   YawBrMass   - Yaw bearing mass (kg)
1.2919E+07   PtfmMass    - Platform mass (kg)
7.5534E+09   PtfmRIner   - Platform inertia for roll tilt rotation about the platform CM (kg m^2)
8.2236E+09   PtfmPIner   - Platform inertia for pitch tilt rotation about the platform CM (kg m^2)
1.3612E+10   PtfmYIner   - Platform inertia for yaw rotation about the platform CM (kg m^2)
```

Figure 23:OC5 ElastoDyn

The mooring input file for the dynamic modelling with MoorDyn is adjusted according to the mooring lines used in the experiment. The three lines are not exactly similar according to Robertson et al [37]. Even though NREL suggests to model the lines similarly with averaged values, this thesis treats them as individual [35]. Therefore, each line is modeled separately to capture the slight differences in Young's moduli and mass densities between the lines. Figure 24 shows the input file for MoorDyn:

```
---------------------- MoorDyn Input File ------------------------------------
Mooring system for OC4-DeepCwind Semi
FALSE    Echo      - echo the input file data (flag)
---------------------- LINE TYPES --------------------------------------------
3        NTypes    - number of LineTypes
Name     Diam      MassDen      EA     BA/-zeta  Can   Cat   Cdn   Cdt
(-)       (m)      (kg/m)       (N)    (N-s/-)   (-)   (-)   (-)   (-)
main     0.1369    125.60     7.520E8  -1.0      0.8   0.25  2.0   0.4
main     0.1398    125.80     7.461E8  -1.0      0.8   0.25  2.0   0.4
main     0.1393    125.40     7.478E8  -1.0      0.8   0.25  2.0   0.4
---------------------- CONNECTION PROPERTIES ---------------------------------
6       NConnects - number of connections including anchors and fairleads
Node     Type      X        Y        Z       M     V      FX   FY   FZ   CdA   CA
(-)      (-)      (m)      (m)      (m)     (kg)  (m^3)  (kN) (kN) (kN) (m^2)  (-)
1       Fixed   418.8    725.383  -200.0     0      0      0    0    0    0     0
2       Fixed  -837.6      0.0    -200.0     0      0      0    0    0    0     0
3       Fixed   418.8   -725.383  -200.0     0      0      0    0    0    0     0
4       Vessel   20.434   35.393   -14.0     0      0      0    0    0    0     0
5       Vessel  -40.868    0.0     -14.0     0      0      0    0    0    0     0
6       Vessel   20.434  -35.393   -14.0     0      0      0    0    0    0     0
---------------------- LINE PROPERTIES ---------------------------------------
3        NLines     - number of line objects
Line     LineType  UnstrLen  NumSegs   NodeAnch  NodeFair  Flags/Outputs
(-)       (-)       (m)       (-)       (-)       (-)         (-)
1         main     835.5      20        1         4           -
2         main     835.5      20        2         5           -
3         main     835.5      20        3         6           -
---------------------- SOLVER OPTIONS ----------------------------------------
0.001    dtM       - time step to use in mooring integration (s)
3.0e6    kbot      - bottom stiffness (Pa/m)
3.0e5    cbot      - bottom damping (Pa-s/m)
2.0      dtIC      - time interval for analyzing convergence during IC gen (s)
60.0     TmaxIC    - max time for ic gen (s)
4.0      CdScaleIC - factor by which to scale drag coefficients during dynamic relaxation (-)
0.01    threshIC  - threshold for IC convergence (-)
```

Figure 24: MoorDyn file for OC5

The first line of tests is performed with a hybrid model of Potential Flow theory enhanced with Morison's equation. Afterwards a Morison's equation-only model is used to obtain detailed information about the difference in both approaches. Both approaches are in the following marked by the ending respective endings *"_PF"* and *"_ME"*.

4.2.1.2 Model using Morison's equation

The model using Morison's equation only differs in the HydroDyn input file. All Potential Flow contribution coming from WAMIT are set to zero in the WAMIT files. Then the ME model is implemented by adding added mass, added drag and dynamic pressure coefficients for each structure element according to table 7:

Table 7: Hydrodynamic parameters of the OC5 system

Added-mass coefficient (C_a) for all members	0.63
Added-mass coefficient (C_{az}) for base column in z-direction	1.0
Drag coefficient (C_d) for main column	0.56

Drag coefficient (C_d) for upper columns	0.61
Drag coefficient (C_d) for base columns	0.68
Drag coefficient (C_d) for pontoons and cross members	0.63
Drag coefficient (C_{dz}) for base columns in z-direction	4.8
Axial dynamic pressure coefficient	1.0

The values are taken from the OC4 system which features a similar platform geometry as the OC5 platform. The added-mass coefficient is calculated by setting $C_a \rho V$ equal to the zero-frequency limit of the surge and sway elements in the WAMIT added-mass matrix. The drag-coefficients are dependent on the Reynold's number and therefore vary with the incoming waves. The used values are averages of the coefficients for the geometry and expected flow regimes of the platform. An axial dynamic pressure coefficient of 1 was applied to all members. More information about the derivation of the values can be found in the definition of the OC4 semisubmersible platform [12].

4.2.2 Model calibration

To ensure the floating system is modelled properly in FAST, a series of static equilibrium and free decay tests as a calibration phase is performed. The models are repeatedly adjusted and fine-tuned in order to achieve results that resemble the experimental measurements as closely as possible. This is necessary due to uncertainties regarding some properties of the model, like the ballast or the influence of the cable bundle which is transmitting the sensor signals. Additionally, the wave and wind loads needed to be calibrated which was done by the initial participants of the OC5 project and is therefore not part of this thesis [35].

4.2.2.1 Static Equilibrium

The matching of the static end position under no wind or wave influence is the starting calibration step for the FAST models. In the first iteration of the static equilibrium test for both models, the surge displacement was almost zero, which results in to too small tensions in the mooring lines and a higher heave displacement. This is addressed by adding a pretension in positive surge and negative heave direction to match the experimental equilibrium position. The other degrees of motion are also slightly adjusted to match the experimental results as closely as possible. Figure 25 and figure 26 show the results of the first calibration phase.

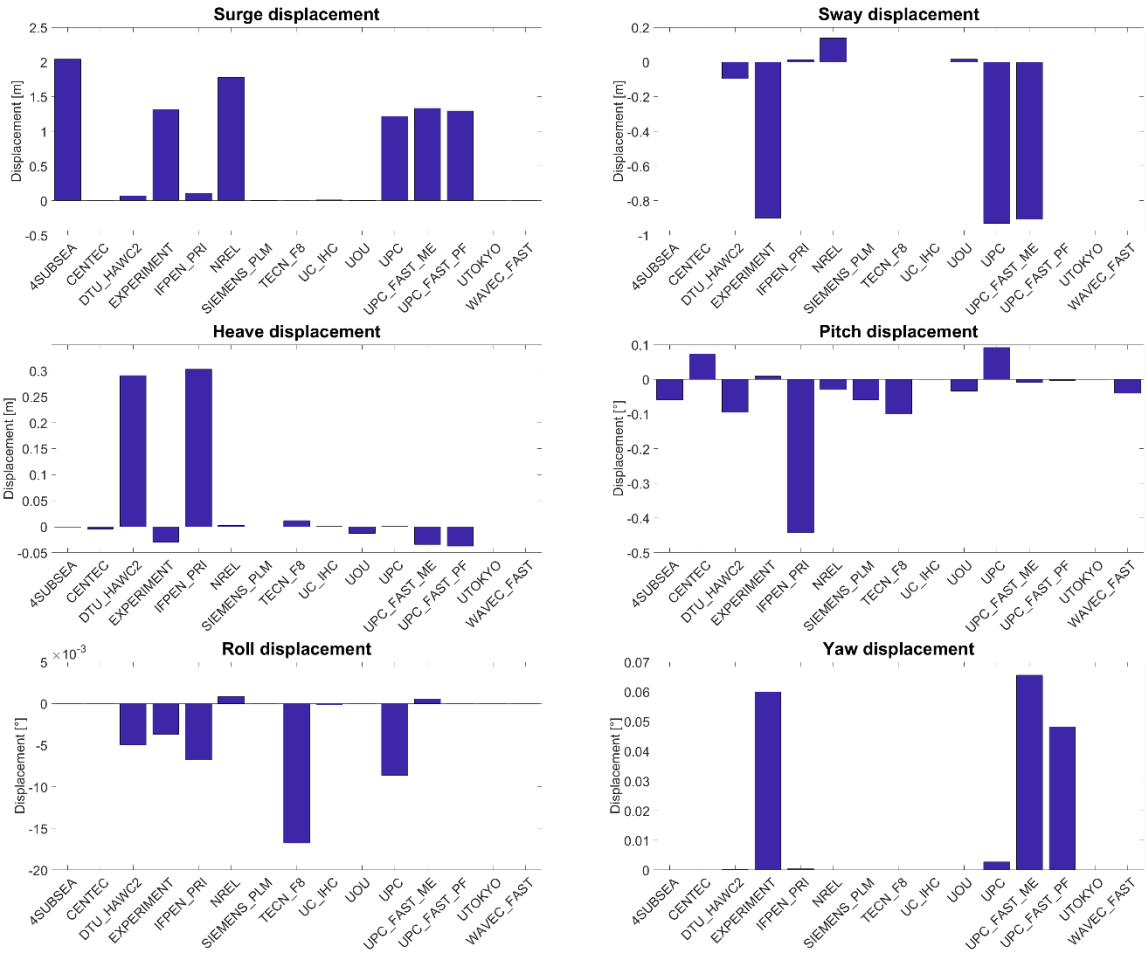

Figure 25: Static equilibrium position of the OC5 system

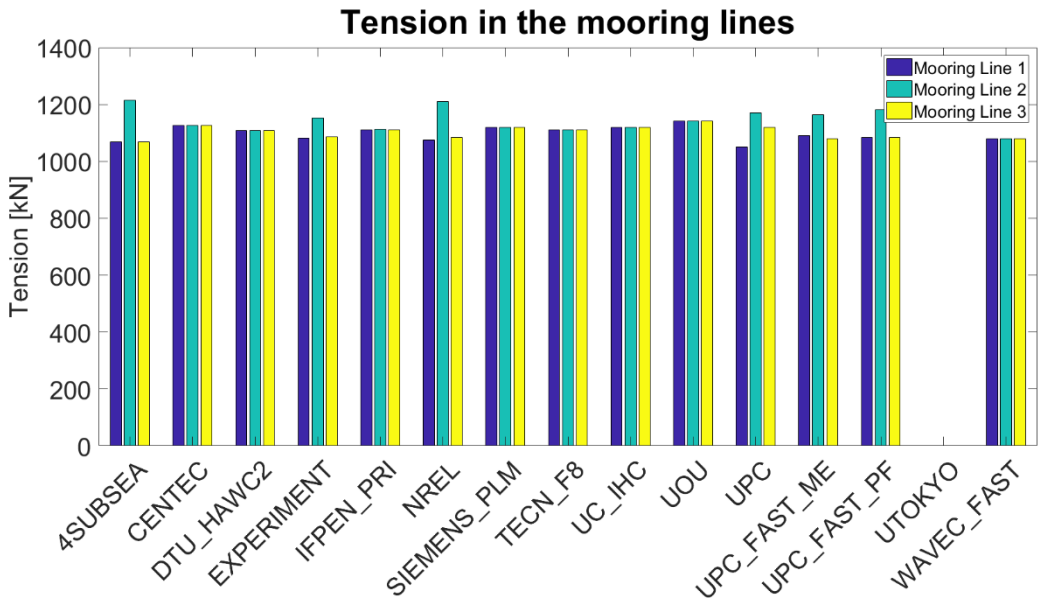

Figure 26: Tension in the mooring lines in equilibrium position

4.2.2.2 Free Decay

After the static equilibrium tests, a series of free decay tests is performed to gain information about the natural frequencies of the platform and the tower. The periods are directly read from the plotted free

decay graph. The results of the FAST models differ slightly from the measured values. In particular the pitch and roll motion show differences up to 2.5 seconds for their periods. The tower model created in Autodesk ROBOT shows a slightly lower stiffness and therefore an increased period compared with the experimental finding.

Table 8 summarizes the findings of the free decay tests:

Table 8: Results of the OC5 free decay tests

DOF	Code	Frequency [Hz]	Period [s]
Surge	Experimental	0.0094	107.00
	FAST_ PF	0.0093	107.50
	FAST_ME	0.0090	110.80
Sway	Experimental	0.0089	112.00
	FAST_ PF	0.0089	111.20
	FAST_ME	0.0087	114.70
Heave	Experimental	0.0571	17.50
	FAST_PF	0.0583	17.17
	FAST_ME	0.0590	16.94
Roll	Experimental	0.0305	32.81
	FAST_PF	0.0336	29.75
	FAST_ME	0.0335	29.84
Pitch	Experimental	0.0308	32.50
	FAST_PF	0.0336	29.75
	FAST_ME	0.0330	30.25
Yaw	Experimental	0.0124	80.80
	FAST_PF	0.0122	81.84
	FAST_ME	0.0120	82.86
Tower bending fore/aft	Experimental	0.315	3.18
	FAST_PF	0.310	3.22
	FAST_ME	0.310	3.22
Tower bending side/side	Experimental	0.325	3.08
	FAST_PF	0.310	3.22
	FAST_ME	0.310	3.22

4.2.3 Behaviour with regular waves

To examine the response of the system to wave excitation, two load cases with regular waves are performed. Load case 31 features a wave height of 7.37 meters and a period of 12.07 seconds. Load case 32 has slightly stronger wave excitation a height of 9.41 meters and 14.3 seconds period. Both load cases are

run without wind influence and only the degrees of freedom for tower and platform enabled. The chosen comparison methods are Response Amplitude Operators for the movements and mooring lines of the system. The RAO are calculated as explained in equation 4 as the ratio of the system's response to the wave excitation. Figure 27 compares the two FAST models with the experimental results for load case 32. Figure 28 shows the findings of the participants of the OC5 project.

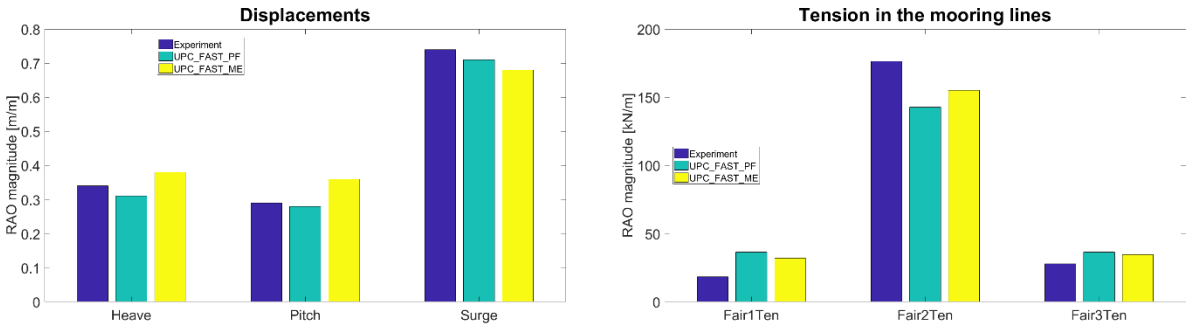

Figure 27: Response Amplitude Operators of the OC5 system for regular waves

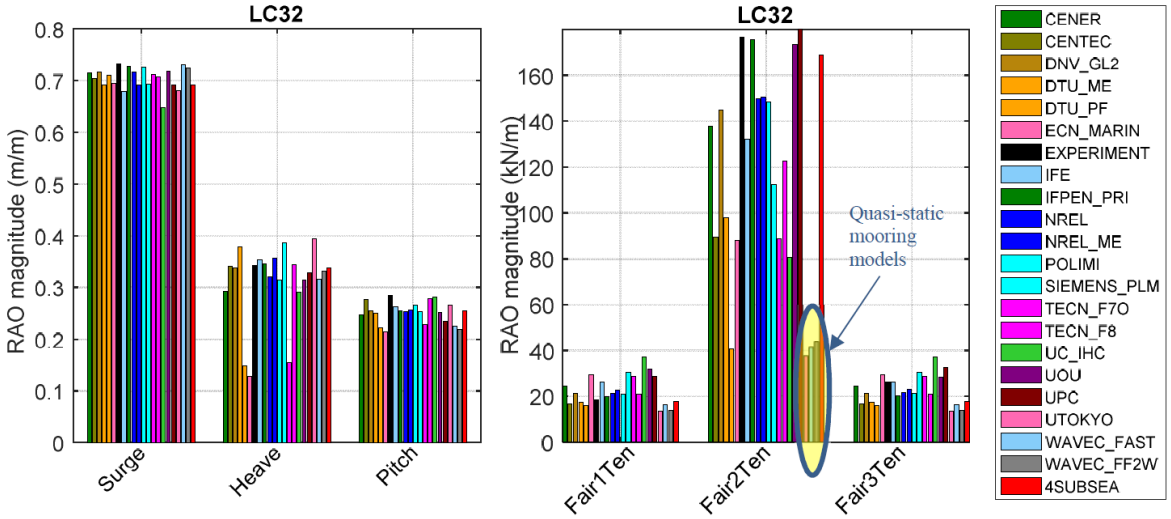

Figure 28: RAOs in load case 32 of the OC5 project [32]

Both models predict the movements well. The ME-only version displays slightly overestimated heave and pitch motions while underpredicting surge displacements. The pitch discrepancy is probably caused by the omitting of the ballasting in the model. Since the ballast data is, as mentioned in chapter 4.2.1, not available, it is included as part of the rigid platform. This leads to a reduced platform inertia due to the concentration of the mass in the center of gravity. The deviations in the surge and heave response are a product of the not-perfectly adjusted hydrodynamic coefficients. Connected to this are the slight mismatches in the mooring response. Both models overpredict the tension in lines one and three while showing too little tension in line two. The results fit well within the range of the participants of the initial study and predict the behavior of the system under regular wave excitation sufficiently well.

4.2.4 Behaviour with irregular waves

Next, a test with an irregular wave field which uses a JONSWAP spectrum with a significant wave height of 7.1 meters, a 12.1 seconds period and a peak shape parameter of 2.2 is performed. A study of the ultimate and fatigue loads on the base of the tower done in the initital OC5 project, discovered a grouping of the used codes.

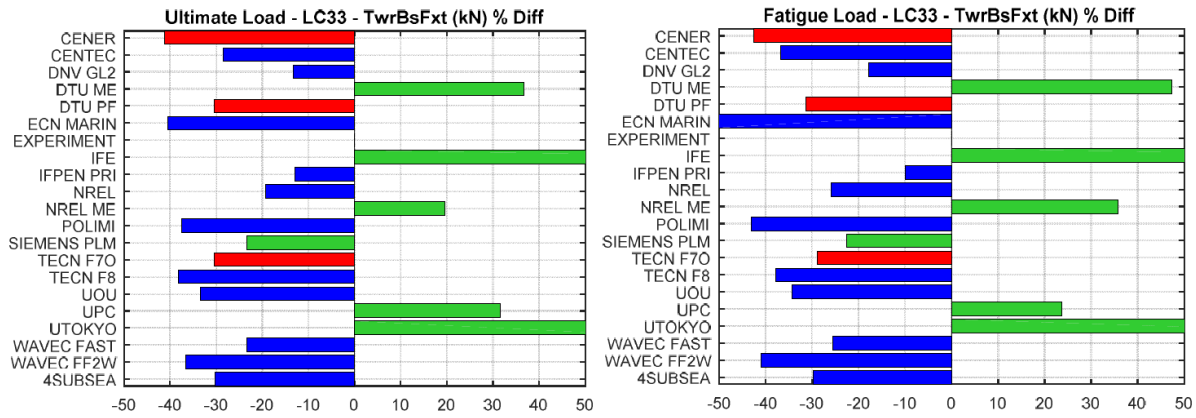

Figure 29: Ultimate and fatigue loads at the tower base [32]

Codes using Potential Flow models are prone to underestimate the occuring loads while Morison's equation-based codes predict too high forces. To find the reason for this disparity, the power spectral density of the load on the tower base is examined.

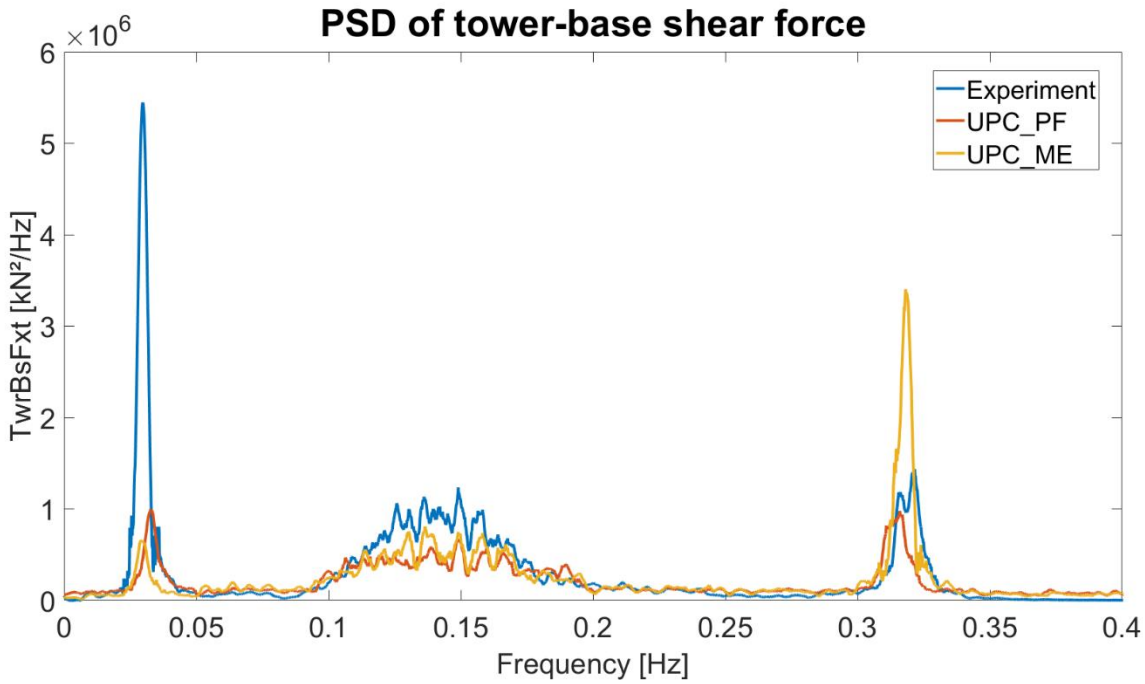

Figure 30: Power spectral density of the tower base loads

Three peaks are observable. The first peak corresponds to the pitch natural frequency of the platform. It is the reason for the underestimation of the load in PF codes. The peaks of the FAST models are slightly shifted to the right due to the difference in the natural pitch periods found in the free decay tests. Between

0.1 and 0.2 Hz is the wave frequency. Both models agree with the excitation of the experiment. The last visible peak happens at the tower natural frequency which is shifted towards lower frequencies due to the decreased stiffness of the used tower model. Here the reason for the load overestimation of the ME code is seen. The code predicts double the peak load compared to the experimental results. The PF code are close to the measured values. The same behaviour is observed in the findings of the participants of the OC5 study. As seen in figure 31, all ME-only codes (marked with dotted lines) heavily overrate the excitation at the tower-bending natural frequency.

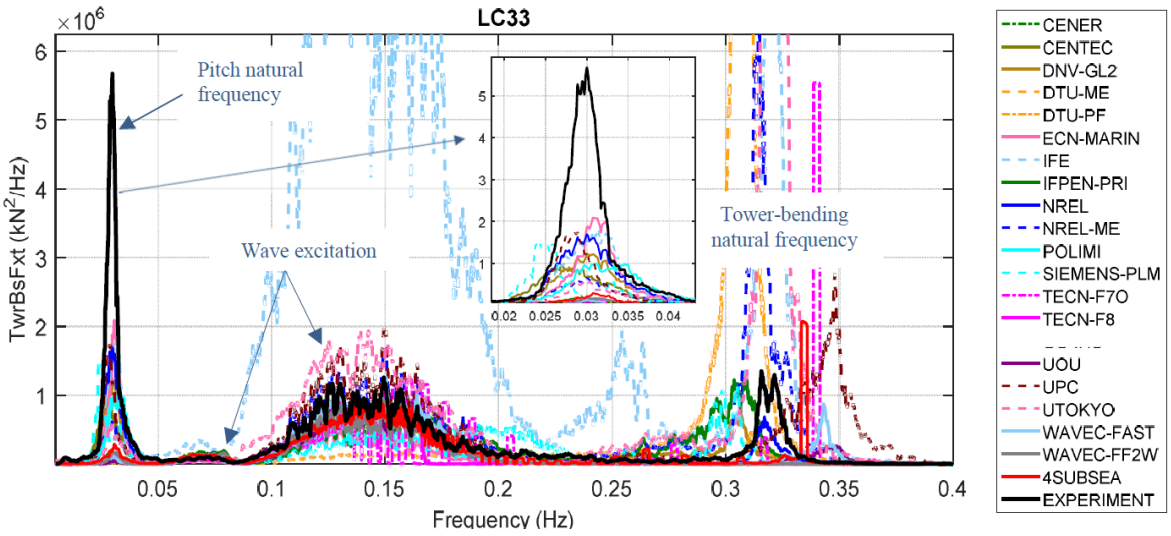

Figure 31: PSD of the tower-base load in load case 3.3 [32]

Several reasons are proposed for this behaviour. Robertson et Al. [32] connect it with the treatment of the added mass while the UPC considers the implementation of diffraction loads responsible for it. Therefore, chapter 5 contains a possible solution to include diffraction loads in Morison's equation by treating the wave field with MacCamy's and Fuchs's diffraction theory.

4.3 Summary

The objective of chapter 4 was to understand the differences in calculating the hydrodynamics of the OC5 system with either a Potential Flow based model or using only Morison's equation. The results are compared with the experimental observations. For this purpose, two different sets of input files for FAST are created. The modified geometry of the turbine is taken into account. Due to limited information about the ballasting of the platform, a simplified approach without filled members is chosen.

First a series of static equilibrium and free decay tests are performed to finetune the models to match equilibrium positions and natural frequencies with the experimental values. The results are sufficiently close for the models. In both models, a surge pretension has to be added to match the experimental displacement in surge direction. Afterwards load cases with regular wave excitation are carried out to evaluate differences in the systems' response. Both models match the experimental values but the ME version shows a pitch overprediction caused by too little inertia due to the modelling of the ballast as part of the rigid platform. Furthermore, a discrepancy in the mooring RAOs is observed with both FAST codes

distributing the loads slightly more evenly between the three mooring lines than in the experiment. Nevertheless, the results are coherent with the finding of the participants in the project and deviate not too far from the experiment. Afterwards, the force on the base of the tower during the excitation of the platform with irregular waves is analysed. The PSD of the response signal is compared. The tests show the same results as for the OC5 participants. All codes underestimate the excitation around the pitch natural frequency of the platform. This leads to PF codes generally underpredicting the ultimate and fatigue loads on the tower base. ME codes show the opposite effect because they additionally tend to forecast significantly increased excitations around the natural tower bending frequency. This overprediction of ME codes might be caused by the disregard of diffraction effects in the calculation of the hydrodynamic response. Chapter 5 offers an approach to solve this problem.

5 MacCamy's and Fuchs's theory of wave diffraction

5.1 Introduction

The last part of the thesis deals with the question if the inclusion of the diffraction theory of MacCamy and Fuchs into codes like FAST will provide a significant improvement of the results, range of conditions and platform types that can be evaluated. So far for diameter to wavelengths ratios smaller than 0.2 ($\frac{D}{\lambda} < 0.2$) Morison's equation or Potential Flow solution is used. For higher wavelengths, wave diffraction becomes and important parameter when the diameter of the column is larger than the average incoming wavelength. FAST approximates the inertial forces in the form of the Froude-Krylov Force in the Potential Flow model and adds diffraction terms via WAMIT [38]. Morison's equation, which delivers less accurate results than Potential Flow-based models for large diameters disregards diffractions terms completely. A possible inclusion of MacCamy's and Fuchs's diffraction theory could enable Morison's equation even for vessels with large diameters. The theory that they presented in 1954 describes the diffraction forces on embedded, vertical, circular cylinders in water of finite depth. Figure 32 shows the typical pattern of a scattered wave in proximity of such a cylinder.

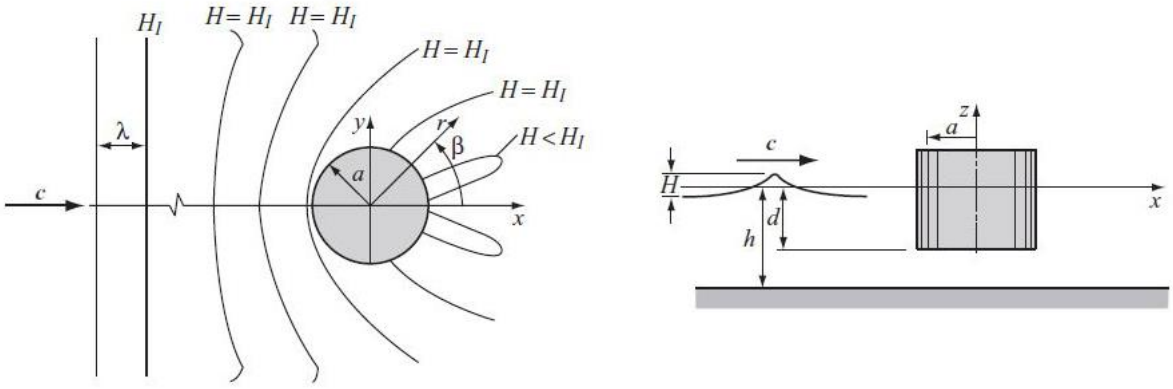

Figure 32: Cylinder in diffracted wave field

The wave is reflected on the front of the cylinder, between an angular range of $\frac{\pi}{2} < \beta < \frac{3\pi}{2}$. The reflected wave loses energy while moving radially away from its point of origin. Thus, the highest point of the reflected wave occurs at $\beta = \pi$ while approaching 0 at $\frac{\pi}{2}$ and $\frac{3\pi}{2}$. Behind the cylinder, between $\pm\frac{\pi}{2}$, the wave energy is transmitted into the wave shadow zone which is shielded from the direct wave incidence.

5.2 Mathematical derivation of the force on an embedded cylinder

The following explanation is valid for a bottom-fixed cylinder. To calculate the force the wave exerts on the cylinder, MacCamy and Fuchs assume that the flow field is a potential flow field, meaning it is irrotational and viscous effects and other losses are negligible. With these assumptions, the velocity potential of the wave can be described as the sum of the incident wave (φ_I) and the reflected wave pattern (φ_D).

$$\varphi_{tot} = \varphi_I + \varphi_D \tag{10}$$

The velocity potential of the linear incident wave, which travels in positive x direction (see figure 1 for the coordinate systems) can be described with:

$$\varphi_I = \frac{H_I}{2}\frac{g}{\omega}\frac{\cosh[k(z+h)]}{\cosh(kh)}\sin(kx - \omega t) \tag{11}$$

k = wave number
h = draft of the cylinder
H_I = height of incoming wave
ω = wave frequency

The following mathematical part is a short summary on how to calculate the force and overturning moment due to incident waves on the cylinder. Detailed explanations and discussions about the involved math is found in MacCamy and Fuchs (1954) [39] and McCormick (2010) [18]. Equation 11 can be transformed into polar coordinates and expressed by using Bessel functions. This allows for the separation of temporal and spatial parts and results in the following expression:

$$\varphi_I = -\frac{H_I}{2}\frac{g}{\omega}\frac{\cosh[k(z+h)]}{\cosh(kh)}\Re\left\{\sum_{m=0}^{\infty} i^{m+1}\varepsilon_m J_m(kr)\cos(m\beta)\, e^{-i\omega t}\right\} \tag{12}$$

ε_m is called the Neumann's symbol and is defined as 1 for m=0 and 2 for all other cases. The symbol $\Re$ signifies that only the real part of the term in brackets is considered. $J_m(kr)$ is the n-th-order Bessel function of the first kind. A mathematical discussion about Bessel functions is available in the books by Abramowitz and Stegun (1965) and Gradshteyn and Ryzhik (1965).

The diffracted wave's velocity potential must fulfil Laplace's equation in cylindrical coordinates:

$$\nabla^2(\varphi_D) = \frac{1}{r}\frac{\partial}{\partial r}\left(r\frac{\partial \varphi_D}{\partial r}\right) + \frac{1}{r^2}\frac{\partial^2 \varphi_D}{\partial \beta^2} + \frac{\partial^2 \varphi_D}{\partial z^2} = 0 \tag{13}$$

The equation is solved using a separation of variables. Together with the seafloor boundary conditions, the velocity potential for the diffracted wave can be formulated as:

$$\varphi_D = \frac{H_I}{2}\frac{g}{\omega}\frac{\cosh[k(z+h)]}{\cosh(kh)}\Re\left\{\sum_{m=0}^{\infty} i^{m+1}E_m H_m^{(1)}(kr)\cos(m\beta)\, e^{-i\omega t}\right\} \tag{14}$$

E_m is a constant connected to the value of m. $H_m^{(1)}(kr)$ is called the m-th-order Hankel function of the first kind. Inserting the equations for the incoming and diffracted velocity potential into equation 10 yields the total velocity potential of the wave field:

$$\varphi = \frac{H_I}{2}\frac{g}{\omega}\frac{\cosh[k(z+h)]}{\cosh(kh)}\Re\left\{\sum_{m=0}^{\infty}\left[-i^{m+1}\varepsilon_m J_m(kr) + E_m H_m^{(1)}(kr)\right]\cos(m\beta)\, e^{-i\omega t}\right\} \tag{15}$$

To find the values of the missing variable E_m, the boundary condition for the cylinder surface is used. Since we consider a irrotational field, the flow across the surface is zero. Therefore, the following condition applies:

$$\frac{\partial \varphi}{\partial r}|_{r=a} = 0 \tag{16}$$

Solving this pair of equations results in:

$$E_m = \varepsilon_m i^{m+1} \frac{J'_m(ka)}{H_m^{(1)'}(ka)} \tag{17}$$

ε_m is again Neumann's symbol and $J'_m(ka)$ and $H_m^{(1)'}(ka)$ the derivative of the Bessel and Hankel function in regard to r. Now that the velocity potential is defined, we can formulate the equation for the dynamic pressure on the cylinder surface. With the help of the linearized Bernoulli's equation for linear waves an expression for the pressure is found by forming the derivative of the velocity potential regarding the time:

$$p|_{r=a} = -\rho \frac{\partial \varphi}{\partial t}|_{r=a} \tag{18}$$

After exchanging the Hankel functions with Bessel functions of first and second kind and further transformations, the pressure can be expressed with equation 19:

$$p|_{r=a} = \rho g \frac{H_I}{2} \frac{\cosh[k(z+h)]}{\cosh(kh)} \Re\left\{\sum_{m=0}^{\infty} i^{m+1} \frac{\varepsilon_m}{H_m^{(1)'}(ka)} \left[\frac{2}{\pi ka}\right] \cos(m\beta)\, e^{-i\omega t}\right\} \tag{19}$$

The last step to obtain the horizontal wave-induced force on the cylinder is the integration of the pressure over the mantel of the cylinder:

$$F_x = -\int_{-h}^{0}\int_{0}^{2\pi} p|_{r=a} \cos(\beta)\, a\, d\beta\, dz \tag{20}$$

Which results in:

$$F_x = 2\frac{\rho g H_I}{k} \tanh(kh) \frac{\sin[\omega t - \sigma(ka)]}{\sqrt{J_1'^2(ka) + Y_1'^2(ka)}} = 2\frac{\rho g H_I}{k} \tanh(kh)\, \Lambda(ka) \sin[\omega t - \sigma(ka)] \tag{21}$$

Λ is the amplitude function and σ the phase angle. The values for these functions can be read from the graphs in figure 33.

Finally, the overturning moment on the cylinder acting in counter-clockwise direction around the y-axis of the structure is given by including the lever arm in the pressure integral:

$$M_y = \int_{-h}^{0}\int_{0}^{2\pi} (z+h) p|_{r=a} \cos(\beta)\, a\, d\beta\, dz = -2\frac{\rho g H_I}{k^3}\left\{kh \tanh(kh) + \frac{1}{\cosh(kh)} - 1\right\} \Lambda(ka) \sin[\omega t - \sigma(ka)] \tag{22}$$

One drawback that should be noted is the inability of the theory to model the effect and influence of diffraction on multiple cylinders. The reflection of the wave on one cylinder influences the wave field around all other members of the platform and vice versa. For now, this thesis neglects this flaw and considers only the diffraction of the wave due to one cylinder.

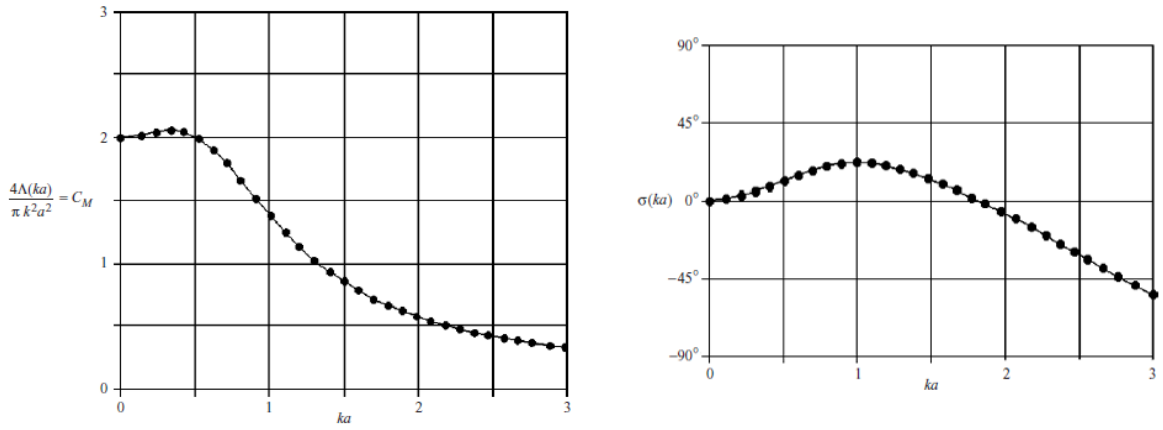

Figure 33: Amplitude function and phase angle depending on the cylinder radius [18]

5.3 Applicability to FAST

To prove the possibility and meaningfulness of adding MacCamy's and Fuchs's theory to established codes, a MATLAB code is developed. The code allows for the creation of a wavefield, which is based on the total velocity potential explained in chapter 5.2. This wavefield already includes reflected waves and therefore the influence of diffraction. The field can then be provided as an external file in the HydroDyn input file. Using this method, Morison's equation can be used to model even platforms with large diameter-to-wavelength ratio.

5.3.1 Code development

The input source of wave fields of FAST can be set to externally generated wave-elevation time series. These input files have two columns, one containing the time and the other the wave elevation. Thus, the MATLAB code needs to create a corresponding output. The wave elevation of a wave field composed of a regular incoming wave and a reflected wave according to MacCamy and Fuchs, is described by the following equation [39]:

$$\eta(r,\beta,t) = \eta_I + \eta_D = -\frac{1}{g}\frac{\partial\varphi}{\partial t}|_{z=0} \tag{23}$$

$$\eta(r,\beta,t) = \frac{H_I}{2}\Re\left\{\sum_{m=0}^{\infty} i^m \varepsilon_m \left[J_m(kr) - \frac{J_m'(ka)}{H_m^{(1)\prime}(ka)} H_m^{(1)}(kr)\right]\cos(m\beta)\, e^{-i\omega t}\right\} \tag{24}$$

The shape of the created wave can be modified by six input parameters:

- Wave height
- Wave period
- Water depth
- Radius of the cylinder
- Simulation time
- Time step for the simulation

The first important parameter is the wave number k. In order to be able to calculate it, first the wavelength λ of the incident wave is needed. It is computed with the help of the dispersion equation:

$$\lambda = \frac{gT^2}{2\pi} * \tanh\left(\frac{2\pi h}{\lambda}\right) \tag{25}$$

Since λ occurs on both sides of the equation, it is solved with an iteration in MATLAB using a starting wavelength of 10m. The selected convergence criterion is 0.001m, which is reasonably exact for the expected wavelengths.

After lambda is found, the wave number is calculated. Subsequently, the sum formula is solved. An investigation of the sum shows, that it converges for m values greater than five. The code uses the first ten terms of the sum formula. For each time step, the sum terms are calculated by evaluating the Bessel functions and their respective derivatives. The terms for m=0...10 are summed up and the function jumps to the next incremental time-step. After multiplication of the real part of the sum with half of the incoming wave height, the results are stored in the wave elevation vector. The resulting wave is a linear regular wave, as the example for a wave (Hs=4m, Tp=8s, h=400m, a=10m) in figure 34 shows. The code also outputs the time of the wave field in a similar vector. These vectors are converted into two columns of a *.elev* text document which is used as the input file for the HydroDyn module of FAST. In Appendix B.1 the full code is depicted.

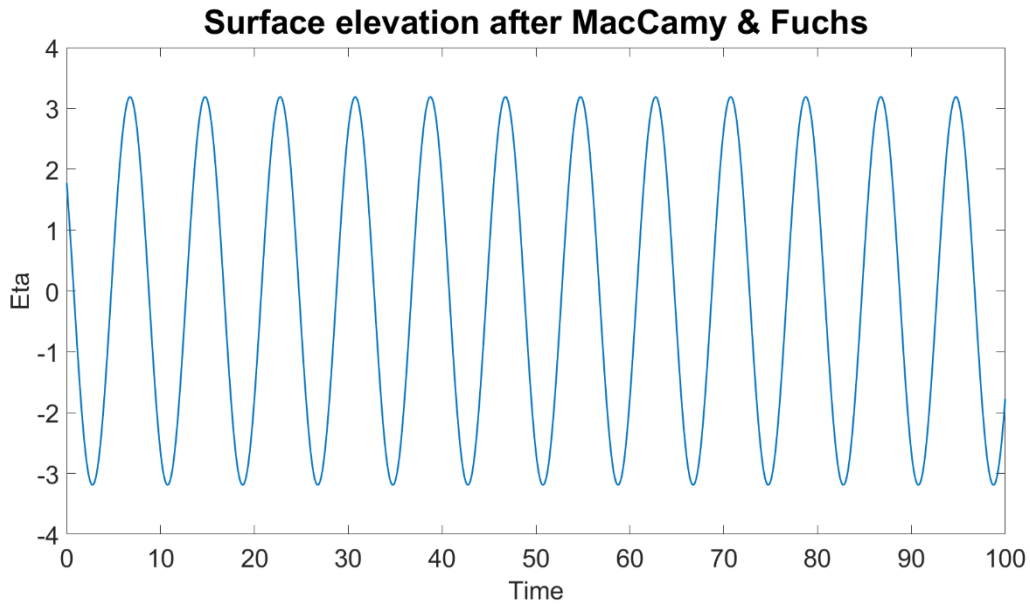

Figure 34: Surface elevation after MacCamy & Fuchs

5.3.2 Application and comparison with Potential Flow models

To validate the correct implementation of the model in MATLAB, several steps are performed. Firstly, the force according to MacCamy and Fuchs on a circular cylinder of ten-meter radius is calculated in MATLAB via formula 23 from chapter 5.2. This value is compared to the results obtained by inserting the wave acceleration of airy waves into the inertia force term of Morison's equation.

The considered water depth is ten meters with a wave height of 2 meters. The wave period is varied to obtain wavelength-to-diameter ratios that are inside as well as outside of diffraction-dominant conditions. The transition happens for the used parameters (10m water depth, 10m radius) at a wavelength of 62.5m according to figure 35, which shows the border between inertia and diffraction regime:

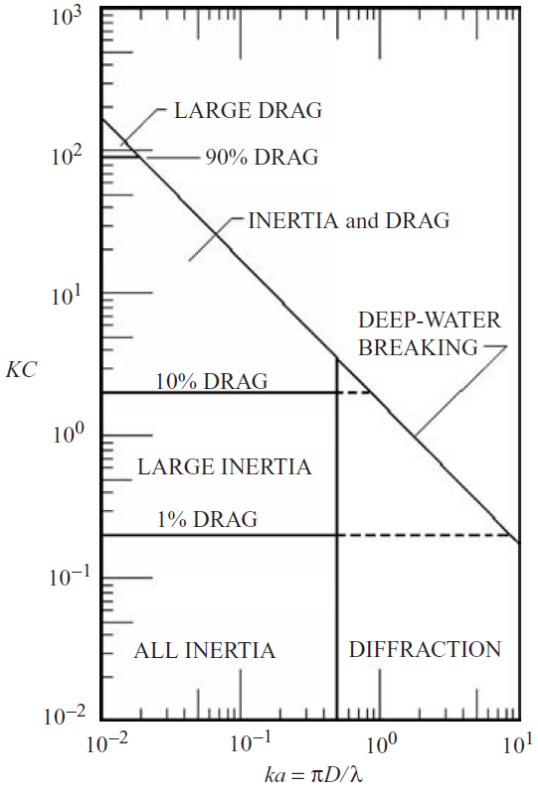

Figure 35: Force component realms [18]

The inertia force exerted by the wave field on the cylinder according to Morison's equation is calculated by integrating the force per unit length from equation 28 alongside the cylinder surface from the still water level to the seafloor:

$$F_{Inertia,Morison} = \frac{\pi}{4}\rho C_m D^2 \cdot \dot{u}(t) \tag{26}$$

As explained in chapter 2.3.1 ρ is the water density, C_m the empiric inertia coefficient, D the cylinder diameter and $\dot{u}(t)$ the wave particle acceleration in x direction.

The acceleration for regular airy waves is given by [18]:

$$\dot{u}(x,z,t) = \frac{H_I \omega^2}{2}\frac{\cosh[k(z+h)]}{\sinh(kh)}\cos(kx-\omega t) \tag{27}$$

The resulting force on the cylinder is achieved by integrating Morison's equation along the cylinder surface. The force predicted by MacCamy and Fuchs and the force resulting from equation 28 with the acceleration from the airy wave field, are plotted together for different wave conditions. Figure 36 and figure 37 present the surface elevations and the forces on the cylinder for different wavelengths:

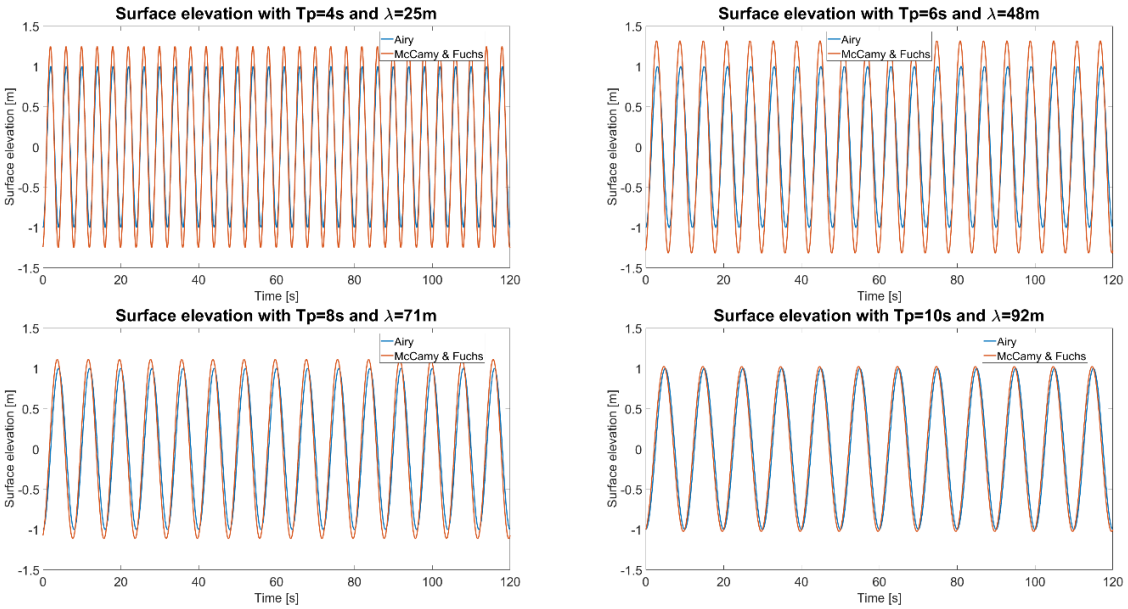

Figure 36: Comparison of the surface elevations for different wavelengths

As figure 36 shows, the predicted wave elevation of MacCamy and Fuchs changes with the wavelength of the incident wave. In cases when the wavelength is short compared to the diameter and diffraction is the dominant force (here for λ<62.5m), the surface elevation has a larger amplitude. With larger wavelengths and after passing the threshold into the inertia-dominated domain, the diffracted wave resembles more and more airy waves. The same phenomena can subsequently be seen in the force on the cylinder. For smaller wavelengths, the force according to MacCamy and Fuchs is significantly smaller than the forces predicted for airy waves with Morison's equation. If the wavelength threshold is surpassed, MacCamy's and Fuchs's theory loses its validity and can no longer be used to predict the force on the cylinder.

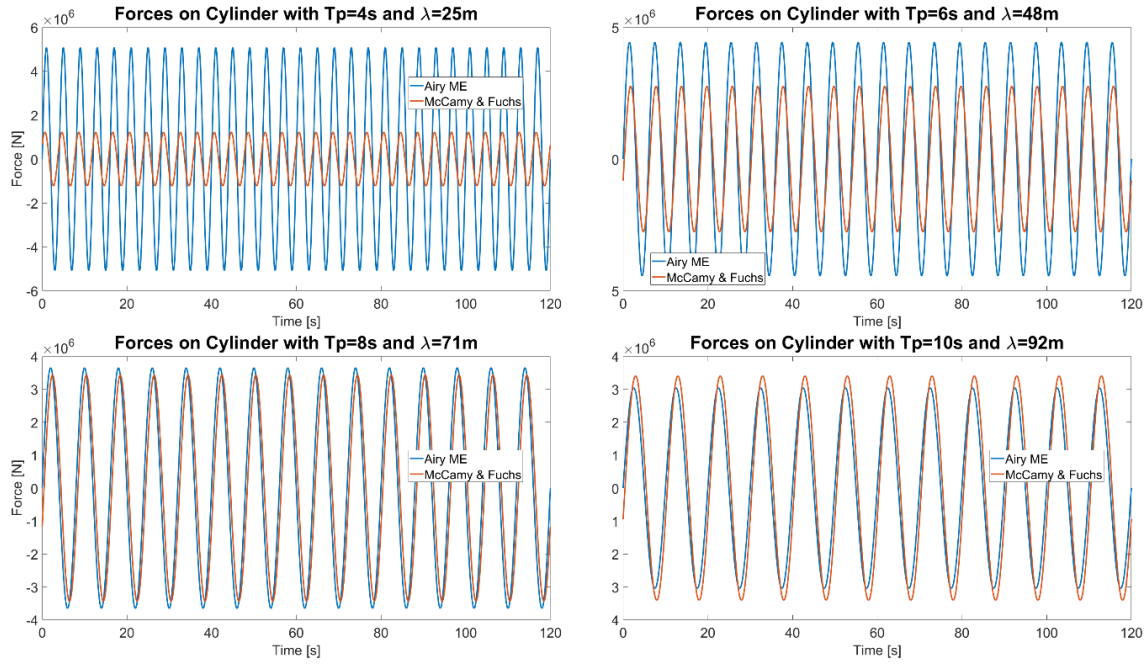

Figure 37: Comparison of the resulting forces for different wavelengths

5.4 Outlook regarding the OC5 study

Chapter 4 showed that there are significant differences in the response of systems like the semisubmersible platform of the OC5 project depending on the hydrodynamic model. An analysis of the Power Spectral Density of ME-only models and models using PF show big disparities. Especially the shear force at the tower base in higher frequency regions is heavily overpredicted by using ME-only models compared to experimental results. This could be caused by the neglected inclusion of diffraction loads. Using a wavefield that is modified according to MacCamy's and Fuchs's diffraction theory in this high frequency spectrum could help to reduce the loads predicted by ME codes. The implementation and validation of this theory would have exceeded the scale of this thesis but can be the topic of future papers.

6 Summary and conclusion

Floating offshore turbines are a relatively new technology suitable to further shift the energy production towards renewable resources. They are designed and analysed using aero-hydro-servo-elastic codes which are able to calculate the complex loads influencing these systems. This thesis uses one of those, FAST 8.16, developed by the National Renewable Energy Laboratory (NREL), to examine the influence of several modelling approaches on the responses of platforms. The NREL participates in several research projects with other institutes, industry and universities called Offshore Code Comparison Collaboration (OC3, OC4 and OC5). OC3 and OC4 aim to benchmark and improve available codes based on theoretical systems while OC5 uses experimental data with a model and compares the response of the codes with it.

After a short introduction in the first chapter, the underlying principles for floating structures are discussed. The differences between bottom-supported and floating systems are highlighted with a short explanation of the employed structure types for both types. Then the underlying hydrodynamic theories, Potential Flow and Morison's equation are explained together with their range of application. The three occurring types of aerodynamic loads, steady, periodic and turbulence loads, are briefly reviewed before a comparison of quasi-static and dynamic mooring models is drawn. The second chapter finishes with an overview over the used software FAST and its various modules.

Chapter three deals with the question if mooring dynamics have a large influence on the loads and movements of floating offshore structures under various conditions. For this, the semisubmersible platform from the OC4 project equipped with the NREL 5MW turbine is analysed with both quasi-static and dynamic mooring models. Several load cases from static equilibrium tests, over free decay test up to full load cases featuring wind and wave excitation are performed. The comparison indicates that the dynamic modelling of the mooring system is important, especially for load cases with wind and wave excitation. Quasi-static approaches heavily underpredict the fatigue loads in the mooring lines especially in higher frequencies of excitation. The failure of quasi-static codes to capture this potential source of fatigue damage implies the necessity to model those load cases with dynamic codes. Alongside the findings from the original study, the OC4 project provides valuable information about the strengths and weaknesses of the different codes

Following is an analysis of the differences between models using only Morison's equation and those using a Potential Flow solution. The OC5 project, an experimental study with a 1:50 model of a semisubmersible platform mounted with a modified turbine is chosen for a comparison. Input files of the OC5 turbine are created for each approach and implemented in FAST. The system is finetuned with static equilibrium tests followed by free decay tests. Due to incomplete information about the ballasting, the platform is assumed to contain no filled members. Thus, the natural frequencies of the platform vary slightly from the experimental findings. Then tests with regular and irregular wave excitation are performed. The RAOs of the displacements agrees well with the experiment, while the excitation in the mooring lines shows a more equal distribution between the lines for both models. Afterwards, a load case with an irregular wave pattern is performed. The focus hereby was on the forces on the tower. ME-only codes tend to

overestimate the loads on the tower base while PF solutions show the opposite behaviour. This is caused by an underprediction of both codes of the excitation at the pitch natural frequency, which is compensated by a severe overprediction of ME codes at the tower bending frequency. The reasons for this behaviour is unknown but could be related to the treatment of diffraction by ME codes.

The last chapter examines the possibility of using hydrodynamic models which use only Morison's equation in situations where wave diffraction is the dominant force. This is the case when the diameters of the platform columns are far smaller than the wavelength at the site. MacCamy and Fuchs proposed a model to describe the velocity potential which contains the initial wave and the contribution of the reflected wave. From this velocity potential, it is possible to derive the surface elevation of the modified wave as well as the force it exerts on the column. This theory is used to create wave elevation time series in MATLAB in order to use them as input files in FAST using Morison's equation. To validate the correct implementation, the wave particle acceleration of regular airy waves is inserted into Morison's equation. The resulting force is compared with the force predicted by MacCamy and Fuchs. The results show reduced loads on a cylinder in diffraction-dominant conditions. This theory could in future works be used to reduce the significant overprediction of occurring forces with ME-only codes observed during the study of the OC5 system in chapter 4.

References

[1] P. Vineis, Health without borders: Epidemics in the era of globalization, Springer, Cham, Switzerland, 2017.

[2] A. Berger, Climate Change: Inferences from Paleoclimate and Regional Aspects, first ed., Springer, Dordrecht, 2012.

[3] Information on http://www.wwindea.org/11961-2/, last checked: 12.12.2017

[4] Information on https://windeurope.org/wp-content/uploads/files/about-wind/statistics/WindEurope-Annual-Offshore-Statistics-2016.pdf, last checked: 12.12.2017

[5] Information on https://www.statoil.com/content/statoil/en/what-we-do/hywind-where-the-wind-takes-us.html, last checked: 12.12.2017

[6] J. Journée, W. Massie, Offshore Hydromechanics, Delft, 2001.

[7] J.F. Wilson, Dynamics of offshore structures, secondnd ed., J. Wiley, Hoboken, N.J., 2003.

[8] Information on http://homepage.tudelft.nl/p3r3s/BSc_projects/eindrapport_dorrepaal.pdf, last checked: 12.12.2017

[9] S. Chakrabarti, Handbook of Offshore Engineering, Elsevier Science [Imprint]; Elsevier Science & Technology Books, San Diego, 2005.

[10] Offshore Energy Structures, Springer International Publishing AG, Cham, 2015.

[11] D. Matha, M. Schlipf, A. Cordle, R. Pereira, J. Jonkman, Challenges in Simulation of Aerodynamics, Hydrodynamics and Mooring-Line Dynamics of Floating Offshore Wind Turbines: NREL/CP-5000-50544, 2011.

[12] A. Robertson, J. Jonkman, M. Masciola, H. Song, A. Coulling, A. Goupee, C. Luan, Definition of the Semisubmersible Floating System for Phase II of OC4: NREL/TP-5000-60601, 2014.

[13] A. Robertson, J. Jonkman, F. Vorpahl, W. Popko, T. Larsen, J. Nichols, J. Azcona, T. Nygaard, A. Hansen, Offshore Code Comparison Collaboration Continuation Within IEA Wind Task 30: Phase II Results Regarding a Floating Semisubmersible Wind System: NREL/CP-5000-61154, 2014.

[14] J. Jonkman, Dynamics Modeling and Loads Analysis of an Offshore Floating Wind Turbine: NREL/TP-500-41958, 2007.

[15] E. Dick, Fundamentals of turbomachines, Springer, Dordrecht, 2015.

[16] D. Matha, Model Development and Loads Analysis of an Offshore Wind Turbine on a Tension Leg Platform, with a Comparison to Other Floating Turbine Concepts: NREL/SR-500-45891.

[17] J. Cruz, M. Atcheson (Eds.), Floating offshore wind energy: The next generation of wind energy, Springer, [Cham], 2016.

[18] M.E. McCormick, Ocean engineering mechanics: With applications, Cambridge University Press, Cambridge, New York, 2010.

[19] J. Jonkman, W. Musial, Offshore Code Comparison Collaboration (OC3) for IEA Task 23 Offshore Wind Technology and Deployment: NREL/TP-5000-48191, 2010.

[20] J. Jonkman, G. Hayman, B. Jonkman, R. Damiani, R. Murray, AeroDyn v15 User's Guide and Theory Manual.

[21] J. Jonkman, A. Robertson, G. Hayman, HydroDyn User's Guide and Theory Manual.

[22] R. Damiani, J. Jonkman, G. Hayman, SubDyn User's Guide and Theory Manual: NREL/TP-5000-63062, 2015.

[23] J. Jonkman, Overview of the ServoDyn Control & Electrical-Drive Module, 2014.

[24] J. Jonkman, Overview of the ElastoDynStructural-Dynamics Module, 2013.

[25] T. McCoy, A. Byrne, Ice Load Project Final Technical Report: Creation of a model for interaction of bottom-fixed wind turbines with surface ice for use with common simulation codes, 2014.

[26] K. Thiagarajan, R. Kimball, A. Goupee, M. Cameron, DESIGN AND DEVELOPMENT OF A MULTIDIRECTIONAL WIND-WAVE OCEAN BASIN, Houston, Texas, 2014.

[27] J. Jonkman, W. Musial, S. Butterfield, G. Scott, Definition of a 5-MW Reference Wind Turbine for Offshore System Development: NREL/TP-500-38060, 2009.

[28] Topics in Modal Analysis & Testing, Springer Verlag, 2016.

[29] J. Jonkman, Description of Load Cases for OC4, Phase II, May / 2013.

[30] J. Jonkman, T. Larsen, A. Hansen, T. Nygaard, K. Maus, M. Karimirad, Z. Gao, T. Moan, I. Fylling, J. Nichols, M. Kohlmeier, J. Vergara, D. Merino, W. Shi, H. Park, Offshore Code Comparison Collaboration within IEA Wind Task 23: Phase IV Results Regarding Floating Wind Turbine Modeling: NREL/CP-500-47534, 2010.

[31] J. Jonkman, A. Robertson, M. Masciola, G. Ramachandran, Investigation of Response Amplitude Operators for Floating Offshore Wind Turbines: NREL/CP-5000-58098, 2013.

[32] A. Robertson, OC5 Project Phase II: Validation of Global Loads of the DeepCwind Floating Semisubmersible Wind Turbine: Robertson/ Energy Procedia 00 (2017) 000–000, Trondheim,Norway, 2017.

[33] A. Robertson, OC5 Project Phase I: Validation of Hydrodynamic Loading on a Fixed Cylinder: NREL/CP-5000-63567, 2015.

[34] Information on http://www.marin.nl/web/file?uuid=05bec777-cb90-4635-89ae-9935c174ec54&owner=350ebb3a-321f-4db6-9fb7-331cfd07b7c0, last checked: 12.12.2017

[35] A. Robertson, J. Jonkman, F. Wendt, A. Goupee, H. Dagher, Definition of the OC5 DeepCwind Semisubmersible Floating System.

[36] A. Jain, A. Robertson, J. Jonkman, A. Goupee, R. Kimball, A. Swift, FAST Code Verification of Scaling Laws for DeepCwind Floating Wind System Tests: NREL/CP-5000-54221, 2012.

[37] A. Robertson, J. Jonkman, F. Wendt, A. Goupee, H. Dagher, Definition of the OC5 DeepCwind Semisubmersible Floating System.

[38] Information on http://web.mit.edu/13.021/demos/lectures/lecture21.pdf, last checked: 12.12.2017

[39] R. MacCamy, R. Fuchs, WAVE FORCES ON PILES: A DIFFRACTION THEORY.

[40] P. Passon, M. Kühn, J. Jonkman, S. Butterfield, T. Camp, T. Larsen, OC3 – Benchmark Exercise of Aero-Elastic Offshore Wind Turbine Codes: NREL/CP-500-41930, 2007.

[41] J. Jonkman, S. Butterfield, J. Nichols, T. Camp, T. Larsen, A. Hansen, J. Azcona, A. Martinez, X. Munduate, F. Vorpahl, S. Kleinhansl, M. Kohlmeier, T. Kossel, C. Böker, D. Kaufer, Offshore Code

Comparison Collaboration within IEA Wind Annex XXIII: Phase III Results Regarding Tripod Support Structure Modeling: NREL/CP-500-44810, 2009.

Appendix A: OC3

A.1 Overview

The Offshore Code Comparison Collaborative (OC3) is a joint project of several research institutes and companies under the leadership of the NREL. Its goal is the comparison of different design codes used to design and model offshore wind turbines. These codes combine conventional, proven codes for land based turbines (aerodynamic, wind-inflow, control systems and structural-dynamic models) with the additional requirements for offshore based systems (waves, current, hydrodynamics, and foundation dynamics). OC3 aims to certify these aero-hydro-servo-elastic codes and examine their robustness and reliability with a focus on the support structure dynamics [19]. An overview over the participants and the codes they used is provided table 9 [19]:

Table 9: Participants and used codes in OC4

FAST	FLEX5	Bladed	Bladed Multibody	ADAMS	SIMPACK	HAWC	HAWC2	BHawC	ADCoS-Offshore
Code Developer									
NREL	DTU	GH	GH	MSC + NREL	SIMPACK + SWE + NREL	Risø	Risø	Risø + Siemens	ADC + IWES
OC3 Participant									
NREL + CENER	DONG + SWE + Vestas	CENER + GH	GH	NREL	SWE	DNV + Risø	Risø	Siemens	IWES
Aerodynamics									
(BEM or GDW) + DS	(BEM or GDW) + DS	(BEM or GDW) + DS	(BEM or GDW) + DS	(BEM or GDW) + DS	(BEM or GDW) + DS	(BEM or GDW) + DS	(BEM or GDW) + DS	(BEM or GDW) + DS	(BEM or GDW) + DS
Hydrodynamics									
(Airy$^+$ or UD) + ME	(Airy$^+$ or UD or Stream) + ME	(Airy$^+$ or Stream) + ME	(Airy$^+$ or Stream) + ME	(Airy$^+$ or UD) + ME	None	(Airy$^+$ or UD) + ME	(Airy$^+$ or UD) + ME	(Airy$^+$ or UD) + ME	(Airy$^+$ or UD) + ME
Control System (servo)									
DLL, UD, SM	DLL, UD	DLL	DLL	DLL, UD	DLL, UD	DLL, UD	DLL, UD, SM	DLL, UD	DLL, UD
Structural Dynamics (Elastic)									
FEM^P + (Modal / MBS)	FEM^P + (Modal / MBS)	FEM^P + (Modal / MBS)	MBS	MBS	MBS	FEM	MBS / FEM	MBS / FEM	FEM
ADC – Aero Dynamik Consult Ingenieurgesellschaft mbH **Airy$^+$** – Airy wave theory; (+) with free surface connections **BEM** – blade-element/momentum **DLL** – external dynamic link library			**DS** – dynamic stall **GDW** – generalized dynamic wake **FEM^P** – finite-element method; (P) for mode preprocessing only **MBS** – multibody-dynamics formulation				**ME** – Morison's equation **MSC** – MSC Software Corporation **SM** – interface to Simulink® with MATLAB® **UD** – implementation through user-defined subroutine available		

The turbine that is used for the OC3 benchmarks is the standardized NREL 5 MW turbine described in chapter 3.2.1. All its properties including rotor aerodynamic properties; blade, drive train, nacelle, and tower structural properties; and generator-torque and blade-pitch control system properties are similar for all participants. The controller is provided by NREL in form of a DLL file. Moreover, everybody uses the same input files for the wind conditions and the wave kinematics to exclude the errors that can be introduced by differences in the wave theories, turbulence models and other stochastic deviations [40].

Project phases

The OC3 project is subdivided into four phases with regard to the used support structure and varying water depths:

Phase I: Rigid monopile foundation in 20 m water depth

Phase II: Flexible monopile to factor in the soil-pile interaction

Phase III: Tripod substructure in 45 m water depth

Phase IV: Floating spar-buoy in 320 m water depth [41]

In general, the examined codes of all participants showed great similarities in the results. The detailed findings including explanations for the differences of the benchmarked codes for each phase can be found in the report NREL/TP-5000-48191 from J. Jonkman and W. Musial [19].

A.2 Analysis

In order to get familiar with FAST and the various input options, phase IV of the OC3 project is selected as a test project. The goal is to reproduce as closely possible the results of the original study. The FAST version used in this report is FAST 8.16 which is a significantly newer version than the one used by the participants of OC3.

Phase IV uses the 5 MW NREL turbine on top of a floater in spar buoy design based on the "Hywind" concept developed by Statoil of Norway. It is a mature yet simple design for which the platform and mooring system data is provided by Statoil. The floater is slightly modified and adapted by NREL to fit the turbine which differs from the one Statoil uses. The structural properties are listed in table 10 while figure 38 shows the 3D model of the platform [30].

Table 10: Structural properties of the OC3 system

Parameter	Value
Depth to Platform Base Below SWL (Total Draft)	120 m
Elevation to Platform Top (Tower Base) above SWL	10 m
Depth to Top of Taper Below SWL	4 m
Depth to Bottom of Taper Below SWL	12 m
Platform Diameter Above Taper	6.5 m
Platform Diameter Below Taper	9.4 m
Platform Mass, Including Ballast	7,466,330 kg
CM Location Below SWL Along Platform Centerline	89.9155 m
Platform Roll Inertia about CM	4,229,230,000 kg•m2
Platform Pitch Inertia about CM	4,229,230,000 kg•m2
Platform Yaw Inertia about Platform Centerline	164,230,000 kg•m2

Figure 38: OC3 Spar buoy

Within Phase IV several tests are performed. Free decay tests in still water and without the influence of incoming wind of the platform are followed by various load cases with changing control, wind, and wave parameters. For this chapter, the free decay tests, and response tests for the excitation with regular and irregular waves and inflow wind were selected. An overview of the test conditions can be seen in table 11:

Table 11: OC3 load cases

Series Run	DOFs	Wind Condition	Wave Condition	Control Conditions	Sim Length	Initial Conditions
1.4 Free Decay Tests	Platform	No Wind	Still Water	Brake Engaged (Control System Off)	600s	Platform Surge = 21m Platform Sway = 18m Platform Heave = 5m Platform Roll = -10 deg Platform Pitch = 10 deg Platform Yaw = -6 deg Others = 0 for each test
5.1	Platform Tower Drivetrain Blades	Steady, Uniform, No Shear: Vhub = 8m/s	Regular Airy H = 6m T = 10s	Control System Enabled	120s	RotSpeed = 9 rpm Azimuth = 0 deg BldPitch = 0 deg Other = 0
5.2	Platform Tower Drivetrain Blades	Vhub = 11.4m/s Iref = 0.14	Irregular Airy Hs = 6m Tp = 10s	Control System Enabled	600s	RotSpeed = 12 rpm Azimuth = 0 deg BldPitch = 0 deg Other = 0

[19]

A.3 Comparison

Free decay tests

The first step is recreating the free decay tests for the system consisting of platform, turbine and mooring system. The control system is disabled for this task, which equals engaged brakes. Furthermore, the degrees of freedom for the tower have been deactivated, leaving only the platform movement in the three directions free. The platform is then displaced in one direction, released and left at peace until the motion dies out. This process is repeated for all six degrees of freedom.

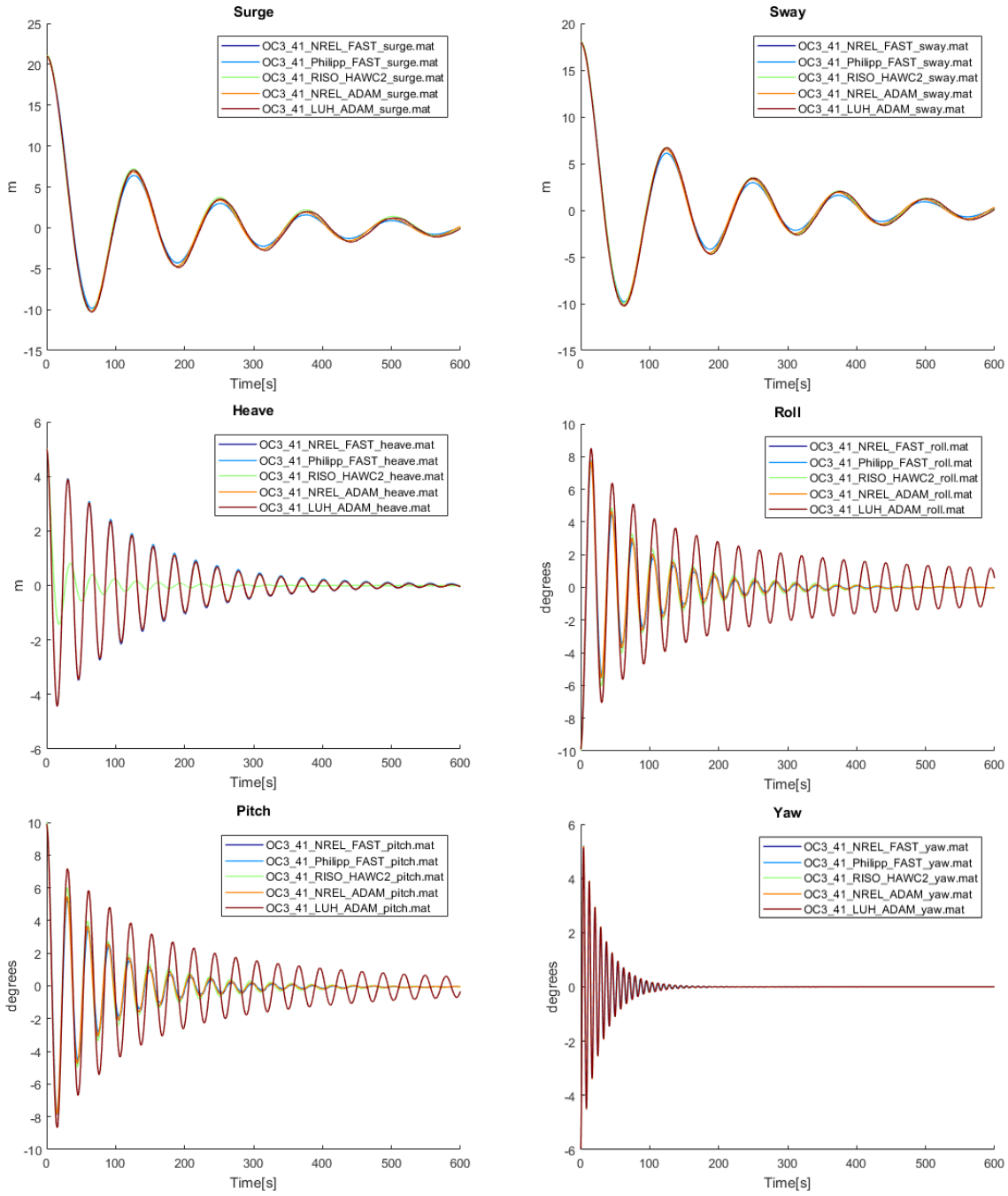

Figure 39: Free decay tests for the OC3 system

The obtained results are mostly similar to those from the NREL (using FAST and ADAM), LUH (also ADAM) and RISØ (using HAWC2). Differences occur for the heave, roll and pitch motion. The heave test of RISØ exhibits significantly smaller amplitudes after the initial displacement and therefore reaches equilibrium conditions quicker than the other models. This can be interpreted as the HAWC2 code predicting more damping compared to the other codes. Furthermore, the roll and pitch motions for LUH show a smaller damping and therefore a bigger amplitude. The results for the used new version of FAST delivers almost identical results to the older version.

Load Case 5.1: Uniform wind and regular waves

Test 5.1 features a steady, uniform wind with a speed of 8 m/s at hub height without any shear. The incoming waves are regular Airy waves with a wave height of 6m and a wave period of 10 s. The turbine has all control systems enabled and runs with an initial rotational speed of 9 rpm. Rotor and drivetrain are modelled flexible. The degrees of freedom for blades, tower, drivetrain and the platform are enabled in this test. The obtained time series results for the motions of the system after the settling of the transients are shown in the following figure.

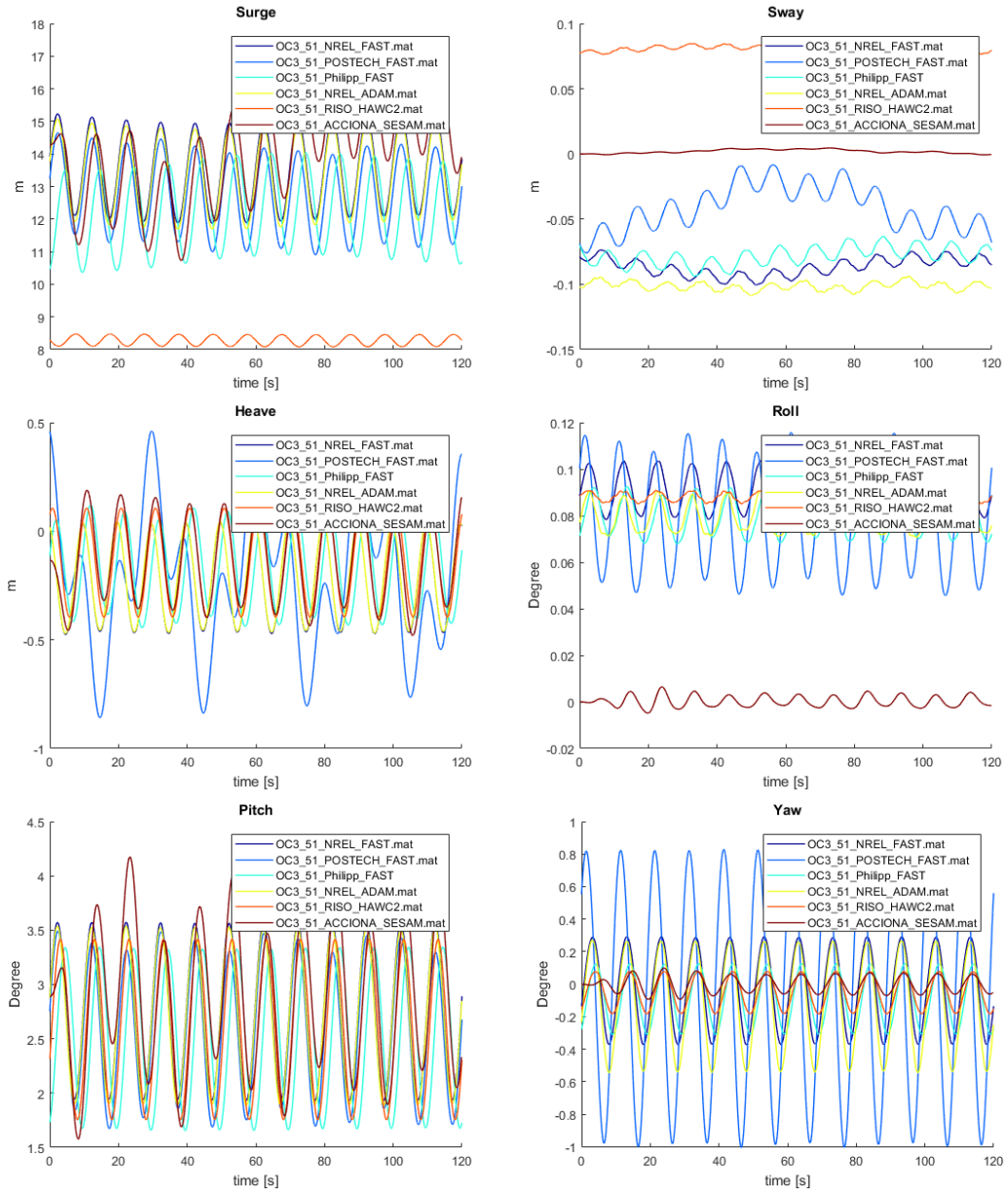

Figure 40: OC3 responses for load case 5.1

The surge motions are, with the exception of the HAWC2 code from RISØ, relatively similar for all participants. HAWC2 predicts a significantly smaller surge with a smaller amplitude. Jonkman et al. argue that the cause for this deviation could simply be the output of wrong parameters [30].

The sway and roll motions are very small with SESAM and HAWC2 showing slightly different behaviour than the other codes. SESAM predicts an almost constant zero sway and roll movement that fluctuates with a small amplitude around the neutral. HAWC2 exhibits a diminished amplitude in both cases. For heave, pitch and yaw the codes mostly agree except for a smaller dampening of POSTECH in the heave and yaw movement and an increased dampening for the yaw movement for HAWC2 and SESAM.

The introduced FAST 8.16 again provides relatively similar results to its older version. It shows the same amplitude for all cases but differs in some cases slightly in the mean value of the oscillation.

A.4 Conclusion

According with Jonkman and Musial [19] the findings of the OC3-Phase IV are listed in this chapter:

Due to the small diameter of the spar shape compared to the occurring wavelengths, the effects of wave diffraction and scattering has only limited influence on the predicted loads and movements for moderate sea conditions. In severe weather and sea states, flow separation might appear alongside the upper part of the platform. Furthermore, radiation damping is insignificant for most modes of motions.

Comparing the theoretical output of the codes with the behaviour of the real Hywind platform, it is found that the hydrodynamic damping needs to be enhanced with additional damping. Linear radiation damping (PF) together with drag terms from ME don't add up to the real values without it.

Several changes had to be made to the control system of the turbine due to the nature of the spar type platform. The natural frequency of the blade-pitch-controller-response was lowered to avoid negative damping during the platforms pitch motion. Additionally, the control criterium after reaching rated power output was switched from constant-power to constant-torque control. This prevents phases of excessive rotor speeds which are enhanced by the change of the blade-pitch controller.

Older versions of FAST and version 8.16 deliver similar results and agree most responses. This shows that even earlier versions of FAST were able to predict the loads and movements on platforms fairly well.

Appendix B: Code for the MacCamy analysis

B.1 Wave Elevation

```
function [WaveElev,Time] = MacCamy_Wave(Hs,Tp,h,a,sim_time,time_step)
%Hs = Waveheight
%Tp = Wave period
%h=water depth
%a=radius cylinder
%sim_time=time wanted for wave field
%time_step=time step for calculations
g=9.80665; %grav. acc
rho=1025; %water density
f=1/Tp; %wave freq
omega=2*pi*f; %ang. freq of wave
n=100; %number terms for sum part
Time=[];
Time=0:time_step:sim_time;
WaveElev=[];
beta=pi;
radius=a;

%% iteration of the wavelenght lambda
lambda=10;

    while abs(g*Tp^2/(2*pi)*tanh(2*pi*h/lambda)-lambda)>0.001
    lambda=g*Tp^2/(2*pi)*tanh(2*pi*h/lambda);
    end

%%
k=2*pi/lambda; %wavenumber

%% Sum part
mod_pot=Hs/2; %value before sum part
rept=0;%part inside the sum
eps_m=1; %neumann's symbol
kr=k*radius;
ka=k*a;

for m=0:length(Time)-1%loop through timesteps
for l=0:n%loop through the sum
    Jm = besselj(l,kr);
    Hm = besselh(l,kr);

    if(l<1)%case analysis for dJm
           dJm=-k*besselj(1,ka);
    else
        dJm=k/2*(besselj(l-1,ka)-besselj(l+1,ka));
    end

        dHm=(l*besselh(l,ka)/a)-(k*besselh(l+1,ka));

    if (l<1)%case analysis neumann's symbold
        eps_m=1;
    else
        eps_m=2;
    end
    %sum
```

```
    rept=rept+((1i^l)*eps_m*(Jm-Hm*(dJm/dHm))*cos(l*beta)*exp(1)^(-
1i*omega*Time(m+1)));

end
WaveElev(m+1)=mod_pot*real(rept);%add surface elevation into array
rept=0;%set sum to 0 for next timestep
end




figure(1)
plot(Time,WaveElev,'linewidth',2)
set(gca,'fontsize',30,'fontweight','demi')
title('Surface elevation after MacCamy & Fuchs','FontSize', 40)
xlabel('Time','FontSize', 30)
ylabel('Eta','FontSize', 30)
```

B.2 Horizontal Force

```
function [F_x,Time] = MacCamy_Force(Hs,Tp,h,a,sim_time,time_step)
%Hs = Waveheight
%Tp = Wave period
%h = water depth
%a = radius of the cylinder
%sim_time = time wanted for wave field
%time_step = time step for calculations
g=9.80665; %grav. acc
rho=1025; %water density
f=1/Tp; %wave freq
omega=2*pi*f; %ang. freq of wave
Time=0:time_step:sim_time ;
F_x=[];



%% iteration of the wavelenght lambda
lambda=10;

    while abs(g*Tp^2/(2*pi)*tanh(2*pi*h/lambda)-lambda)>0.001
    lambda=g*Tp^2/(2*pi)*tanh(2*pi*h/lambda);
    end

%% wavenumber
k=2*pi/lambda;
ka=k*a;
%% amplitude factor 1
mod_force=2*rho*g*Hs*tanh(ka)/(k^2);

%% amplitude factor 2
amp_fct=1/sqrt(((besselj(0,ka)-(1/ka)*besselj(1,ka))^2)+((bessely(0,ka)-
(1/ka)*bessely(1,ka))^2));

%% phase angle
sig=atan((besselj(0,ka)-(1/ka)*besselj(1,ka))/(bessely(0,ka)-
(1/ka)*bessely(1,ka)));
```

```
%% Force
for m=0:length(Time)-1 %loop through timesteps
F_x(m+1)=mod_force*amp_fct*sin(omega*Time(m+1)-sig);
end



 %% Plot

figure(1)
plot(Time,F_x,'linewidth',2)
set(gca,'fontsize',30,'fontweight','demi');
title('Horizontal force after MacCamy & Fuchs','FontSize', 40);
xlabel('Time [s]','FontSize', 30);
ylabel('Force [N]','FontSize', 30);
```